Diagnosing a distributed hydrologic model for two high-elevation forested catchments based on detailed stand- and basin-scale data

Mark Thyer,[1] Jos Beckers,[1] Dave Spittlehouse,[2] Younes Alila,[1] and Rita Winkler[3]

Received 20 June 2003; revised 20 October 2003; accepted 11 November 2003; published 14 January 2004.

[1] This study evaluates the performance and internal structure of the distributed hydrology soil vegetation model (DHSVM) using 1998–2001 data collected at Upper Penticton Creek, British Columbia, Canada. It is shown that clear-cut snowmelt rates calculated using data-derived snow albedo curves are in agreement with observed lysimeter outflow. Measurements in a forest stand with 50% air crown closure suggest that the fraction of shortwave radiation transmitted through the canopy is 0.18–0.28 while the hemispherical canopy view factor controlling longwave radiation fluxes to the forest snowpack is estimated at 0.81 ± 0.07. DHSVM overestimates shortwave transmittance (0.50) and underestimates the view factor (0.50). An alternative forest radiation balance is formulated that is consistent with the measurements. This new formulation improves model efficiency in simulating streamflow from 0.84 to 0.91 due to greater early season melt that results from the enhanced importance of longwave radiation below the canopy. The model captures differences in canopy rainfall interception between small and large storms, tree transpiration measured over a 6-day summer period, and differences in soil moisture between a dry and a wet summer. While the model was calibrated to 1999 snow water equivalent (SWE) and hydrograph data for the untreated control basin, it successfully simulates forest and clear-cut SWE and streamflow for the 3 other years and 4 years of preharvesting and postharvesting streamflow for the second basin. Comparison of model states with the large array of observations suggests that the modified model provides a reliable tool for assessing forest management impacts in the region. *INDEX TERMS:* 1803 Hydrology: Anthropogenic effects; 1818 Hydrology: Evapotranspiration; 1860 Hydrology: Runoff and streamflow; 1863 Hydrology: Snow and ice (1827); 1866 Hydrology: Soil moisture; *KEYWORDS:* snow, radiation, evaporation, soil moisture, streamflow, DHSVM

Citation: Thyer, M., J. Beckers, D. Spittlehouse, Y. Alila, and R. Winkler (2004), Diagnosing a distributed hydrologic model for two high-elevation forested catchments based on detailed stand- and basin-scale data, *Water Resour. Res.*, *40*, W01103, doi:10.1029/2003WR002414.

1. Introduction

[2] Process-based modeling should provide a viable means for evaluating effects of timber harvest on streamflow once such models have been validated against data from small-watershed studies [*Thomas and Megahan*, 1998]. The use of hydrologic models in this respect can alleviate some of the problems associated with statistical analysis of streamflow records by acting as a control to filter out effects of climate variability [*Bowling et al.*, 2000]. Models are also useful for linking forest management impacts measured at the stand level to basin-scale hydrology [*Whitaker et al.*, 2002]. On the other hand, model calibration and uncertainty have long been known to be important concerns [e.g., *Beven and Binley*, 1992]. An important source of model uncertainty stems from a limited quantitative understanding of hydrologic processes in forested watersheds. Any bias or error in the conceptualization of these processes will adversely affect model predictions regarding the hydrologic effects of forestry activities. Only by careful testing with high-quality experimental data describing multiple concurrent internal catchment processes under a range of hydrologic regimes can one determine if a model provides a reliable tool for simulating watershed hydrology or whether improvements to the model structure are needed [*James and Burges*, 1982; *Grayson et al.*, 1992; *Burges*, 2003].

[3] On the basis of the above premises, the distributed hydrology soil vegetation model (DHSVM) [*Wigmosta et al.*, 1994] was applied to two catchments that are part of the Upper Penticton Creek (UPC) Watershed Experiment in the Okanagan region of south central British Columbia (BC) (Figure 1a). This study is part of a larger project aimed at testing the performance of the DHSVM in simulating hydrological processes of forested watersheds across biogeoclimatic zones in BC [*Alila and Beckers*, 2001; *Whitaker et al.*, 2003]. The paired watersheds considered in this study are each approximately 5 km^2 in area, with similar plateau-type topography, soils, and vegetation. Streamflow in these

[1]Department of Forest Resources Management, University of British Columbia, Vancouver, British Columbia, Canada.
[2]Research Branch, British Columbia Ministry of Forests, Victoria, British Columbia, Canada.
[3]Forest Sciences Section, British Columbia Ministry of Forests, Kamloops, British Columbia, Canada.

0043-1397/04/2003WR002414

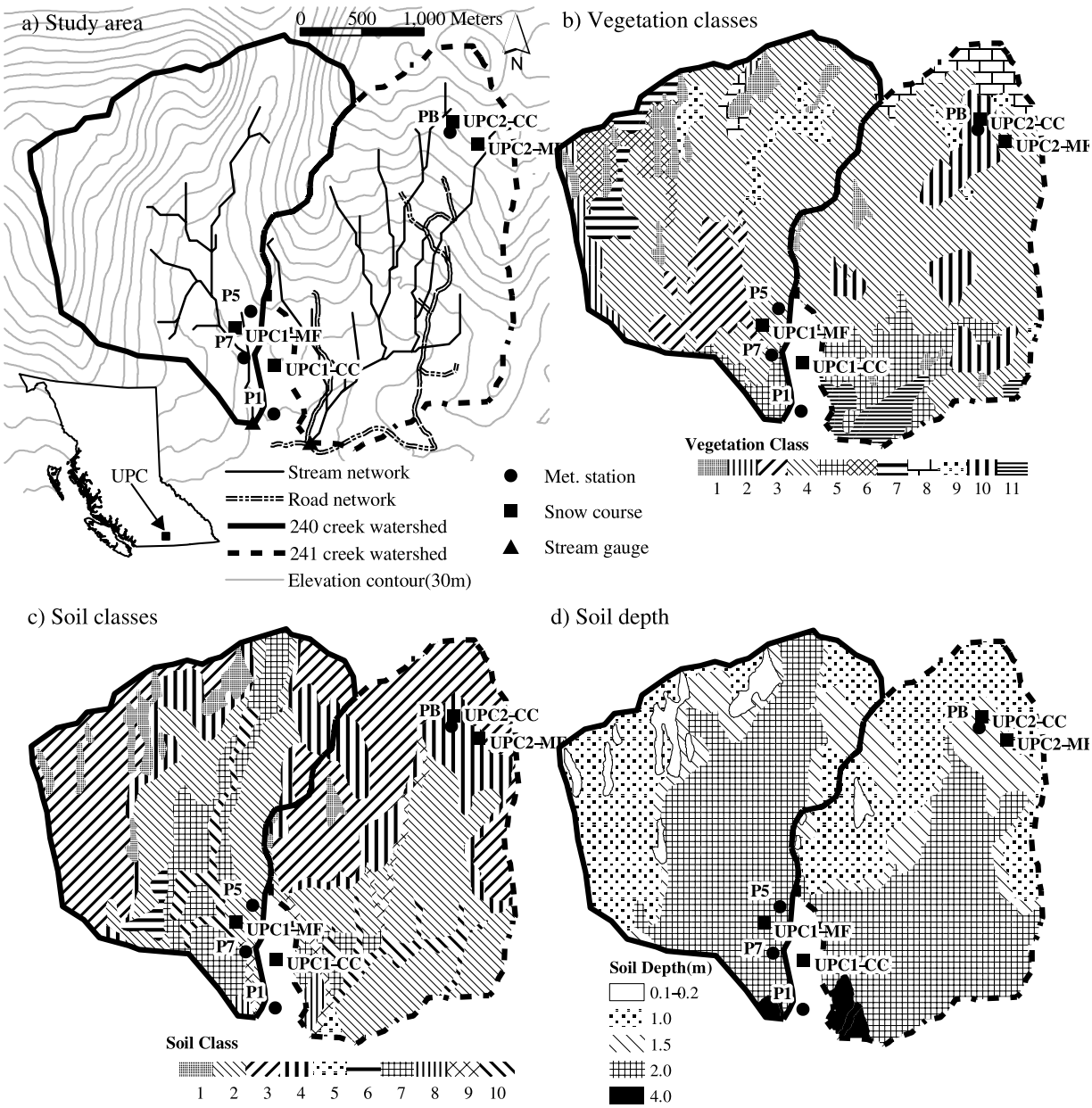

Figure 1. (a) The 240 Creek and 241 Creek catchments. The inset shows the location of the study area in British Columbia. (b) Vegetation classes described in Table 1. (c) Soil classes described in Table 4. (d) Soil depth.

catchments is driven by spring snowmelt. The amount of snow and the timing and rate of snowmelt are strongly influenced by forest cover. The data set for the catchments includes hourly meteorological data and biweekly snow water equivalent (SWE) measurements in two clear-cuts and adjacent forest stands. Ancillary data include measurements of snowmelt in a clear-cut, snow albedo, below-canopy shortwave and longwave radiation, rainfall interception, tree transpiration, and forest and clear-cut soil water content. Hourly streamflow data for both catchments cover the prelogging and postlogging periods, where the 240 Creek catchment has been kept pristine while 241 Creek has so far been 17% clear-cut logged. One of the objectives of this study is to develop and calibrate the model at 240 Creek and evaluate its performance on 241 Creek without recalibration to test the transferability of model parameters between the basins. The richness of observations at UPC provides an opportunity to diagnose the internal performance and structure of the DHSVM in simulating hydrologic responses of high elevation forested catchments in the interior regions of the Pacific Northwest.

[4] During spring snowmelt in south central BC, the snowpack energy balance below mature forest canopies is generally dominated by net radiation [*Adams et al.*, 1998]. Under such conditions, there is good reason to investigate the ability of the model to simulate the forest radiation balance. This will be done by comparing the approach of *Wigmosta et al.* [1994] for simulating the forest radiation

balance with an alternative formulation for canopy shortwave radiation transmittance based on the work of *Pomeroy and Dion* [1996] and a longwave radiation budget based on *Reifsnyder and Lull* [1965]. Another important concern is the suitability of adopted snow albedo curves and the need to make adjustments to represent local conditions [*Blöschl et al.*, 1991]. Leaf litter and protruding vegetation may reduce snow albedo in the forest compared with open areas [*Barry et al.*, 1990; *Hardy et al.*, 1997, 2000]. *Pomeroy and Dion* [1996] note that snow albedo under the canopy was consistent with that in open fields, although it is stated that albedo declined in spring as litter accumulated on the snow surface. Two representations for forest snow albedo will be considered in the UPC model based on alternative hypotheses regarding the effects of needle litter and protruding vegetation on snow reflectance. Finally, soil moisture data and tree transpiration measurements will be used to evaluate model-predicted evaporation.

[5] This paper is organized as follows: Section 2 contains a general overview of the DHSVM including a detailed description of alternative model formulations for representing the forest radiation balance. A description of the UPC study area, measurements, model input, and calibration will be given in section 3. The performance and structure of the calibrated model in simulating hydrologic responses at UPC are evaluated in section 4. The main findings of this evaluation will be summarized in section 5.

2. Distributed Hydrology Soil Vegetation Model (DHSVM)

[6] DHSVM's main features are described below. This description follows closely that of *Storck et al.* [1998], who discuss DHSVM input, output, and calibration in more detail. DHSVM model structure and equations are described in detail by *Wigmosta et al.* [2002]. These model equations are not repeated here except for those processes controlling the accumulation and melt of snow in forested areas that are an important focus of this paper.

2.1. Overview

[7] In DHSVM, the spatial distribution of soil moisture, snow cover, evaporation, and runoff production can be simulated at hourly or longer time steps. The model uses a two-layer canopy representation for interception and evaporation, a two-layer energy-balance model for snow accumulation and melt, a multilayer unsaturated soil model, and a saturated subsurface flow model. Meteorological data input includes precipitation, air temperature, wind, relative humidity, and incoming shortwave and incident longwave radiation. Digital elevation maps (DEMs) are used to model topographic controls on incoming shortwave radiation, precipitation, air temperature, and downslope water movement. Precipitation and air temperature for each model pixel are calculated from point (station) measurements using an elevation gradient approach. The land cover may be composed of overstory vegetation (trees) and/or understory vegetation, or bare soil. The overstory may cover all or a prescribed fraction of the land surface (fractional forest cover F). The understory, if present, is assumed to cover the entire ground surface.

[8] A separate one-dimensional water balance is calculated for each pixel. Precipitation is partitioned into rain and snow based on air temperature and specified values for snow and rain threshold temperatures. DHSVM's canopy snow interception model is based on measurements by *Storck et al.* [2002], where the change in intercepted snow (ΔI) in a certain time step Δt is simulated as a fixed percentage (interception efficiency f) of snowfall (S):

$$\Delta I = f \times S \tag{1}$$

until a maximum interception capacity (m) is reached:

$$I(t + \Delta t) = \min[I(t) + \Delta I, m] \tag{2}$$

Intercepted snow can be removed from the canopy through melt, sublimation, and mass release. Melt of intercepted snow is calculated based on an energy balance approach and results in drip (D). Mass release occurs if sufficient meltwater ($D_{\min}$) is generated during an individual time step such that the snow slides off the canopy, and is simulated as a fixed fraction (M/D ratio) of meltwater drip [*Storck*, 2000]. Drip from the canopy is added to the ground snowpack, if present, as rain, while the cold content of any mass release or nonintercepted snow is accounted for in the ground snowpack energy balance. Ground snow accumulation and melt are simulated using a two-layer energy-balance model, similar to that described by *Anderson* [1968]. The model accounts for net radiation and sensible and latent heat transfers, as well as energy advected by rain, throughfall or drip. Equations for the snow surface shortwave and longwave radiation balance are given in section 2.2.

[9] Rainfall interception is described by equations (1) and (2), with $f = 1$ and with $m = R_m \times \mathrm{LAI}$, where LAI is the overstory or understory leaf area index and where R_m is a rain interception multiplier. Evaporation of intercepted water from the surfaces of wet vegetation is assumed to occur at the potential rate, adjusted for aerodynamic resistance to vapor transport. Transpiration from dry vegetative surfaces is calculated using a Penman-Monteith approach. The model follows *Entekhabi and Eagleson* [1989] in calculating soil evaporation. Vertical unsaturated water movement through the soil layers is calculated using the one-dimensional form of Darcy's law. This downward moisture flux recharges the grid cell water table. Subsurface lateral flow is calculated using a transient, three-dimensional representation of saturated subsurface flow. Return flow and saturation overland flow are generated in locations where grid cell water tables intersect the ground surface. Open-channel routing uses explicit information on the location of stream channels and road ditches and a linear reservoir scheme.

2.2. Forest Radiation Balance

[10] The amount of shortwave radiation absorbed at the snow surface (R_{ss}) is given by [*Wigmosta et al.*, 1994]

$$R_{ss} = (1 - \alpha_s)\tau_c R_s \tag{3}$$

where α_s is the snow albedo or reflection coefficient, and where τ_c is the fraction of incident shortwave radiation R_s transmitted through the forest canopy. On the basis of work

by *Laramie and Schaake* [1972], the snow albedo is given by

$$\alpha_S = \alpha_0 A_a^{(N)^{(B_a)}} \quad (T_S < 0)$$
$$\alpha_S = \alpha_0 A_m^{(N)^{(B_m)}} \quad (T_S = 0) \tag{4}$$

where N is the number of days since the last snowfall event, α_o is the albedo of fresh snow, and A and B are albedo decay coefficients. Different coefficients are used whether the snow is under freezing or melt conditions, as determined by the snow surface temperature, T_s. In this study, distinct sets of albedo curves are also specified for open ($F = 0$) and forested ($F > 0$) areas.

[11] Two alternative representations for calculating the transmittance of shortwave radiation through the canopy will be considered:

$$\tau_c = \tau_i F + [1 - F] \tag{5a}$$

$$\tau_c = \exp\left(-k_F \frac{F}{\sin\theta}\right) \tag{5b}$$

Equation (5a) is DHSVM's original formulation [*Wigmosta et al.*, 1994], in which shortwave radiation transmittance is proportional to the fractional forest cover, and in which τ_i represents the fraction of shortwave radiation transmitted through an individual tree canopy, calculated using a Beer's law relationship:

$$\tau_i = \exp(-k_{\mathrm{LAI}} \mathrm{LAI}_o) \tag{6}$$

where k_{LAI} is an extinction coefficient for the tree canopy, and where LAI_o denotes the projected leaf area index of the overstory (o). Equation (5a) implies that the minimum value τ_c can attain is equal to the fractional open area in a forest stand looking vertically from above [$1 - F$] and assumes that the open area radiation balance is independent of that in the forest. However, with a recommended DHSVM pixel size of 30–100 m [*Storck et al.*, 1998] and tree heights in mature forest stands in the Pacific Northwest ranging from about 20 m (e.g., at UPC) to 50 m in coastal forests, this assumption is not necessarily valid because shading from nearby trees may affect the radiation balance of small forest openings. Equation (5b) provides an alternative approach for calculating τ_c based on the work of *Pomeroy and Dion* [1996] that is not subject to this assumption and which utilizes a Beer's law relationship for an entire forest stand rather than for an individual tree canopy. In (5b), canopy density and the extinction coefficient k_F are defined through F rather than stand LAI because at UPC direct measurements are available for F through forest cover maps whereas LAI is only estimated. Following *Pomeroy and Dion* [1996], the effect of solar angle θ on τ_c is incorporated. In their study, k was also formulated to be a function of solar angle. However, as this $k(\theta)$ relationship is species-dependent and unknown for the UPC forest types, it was taken to be constant.

[12] Alternative formulations are also considered for calculating the longwave radiation exchange at the snow surface L_{ss}:

$$L_{ss} = L_o F + L_d(1 - F) - L_s \tag{7a}$$

$$L_{ss} = L_o V_f + L_d(1 - V_f) - L_s \tag{7b}$$

Both equations depend on downward sky longwave radiation L_d, longwave radiation emitted by the canopy L_o, and the upward longwave flux from the snow surface L_s. These longwave fluxes are calculated from the Stefan-Bolzman equation based on air temperature, canopy temperature, and snow surface temperature, respectively [*Wigmosta et al.*, 1994]. In the original DHSVM formulation (equation (7a)), an independent longwave radiation budget is calculated for the forested and open fractions of a model pixel, using the percent cover of the canopy looking vertically down from above. However, when looking up from the ground or snow surface, a greater proportion of the sky will be blocked from view by the canopy than given by [$1 - F$] and longwave radiation received by the snow surface is better described by a hemispherical view. This rationale leads to an alternative formulation for L_{ss} (equation (7b)) that is a function of the proportion of canopy that is "seen" by the snowpack, the canopy view factor V_f [*Reifsnyder and Lull*, 1965]. Clear-cut ($F = V_f = 0$) simulations are identical for the original (equations (5a) and (7a)) and modified (equations (5b) and (7b)) radiation balance.

3. Study Area, Measurements, and Methods

3.1. Site Description

[13] The study area is part of the UPC Watershed Experiment (49°40′N, 119°24′N) located 26 km northeast of Penticton in south central BC (Figure 1a) [*Winkler et al.*, 2003]. The 240 Creek and 241 Creek catchments each have a drainage area of about 5 km^2, range in elevation from 1600 to 2100 m, and are plateau dominated, with 75% of the study area having slopes less than 30%. Mean annual precipitation at UPC is approximately 750 mm with 50–70% falling as snow. Mean summer (June–August) and winter (November–March) air temperatures are 11°C and −5°C, respectively. Permanent snow cover usually exists from late October until early June. Forest cover is primarily mature lodgepole pine (*Pinus contorta* Dougl.) with lesser amounts of Engelmann spruce (*Picea Engelmannii* Parry) and subalpine fir (*Abies lasiocarpa* (Hook.) Nutt). The understory is composed of mosses, lichens, and shrubs less than 0.5 m tall. Approximately 5% of the 241 Creek basin has been clear-cut logged in the winter of 1995–1996, and an additional 12% was clear-cut logged in 1997–1998, while the 240 Creek control basin has been left undisturbed. The underlying geology consists of massive, largely unfractured and poorly weathered granite, giving a tight water balance with the majority of the water leaving the catchment as streamflow.

3.2. Measurements

3.2.1. Meteorology

[14] Air temperature, precipitation, relative humidity, shortwave radiation, wind speed, and snow and soil tem-

Table 1. Physical Characteristics of Vegetation Classes

Class	Overstory Description[a]	Height,[a] m	Fractional Coverage[a]	Leaf Area Index,[b] m^2/m^2	Understory Present[c]
1	rock	N/A	N/A	N/A	no
2	Lodgepole pine H20	20.1	0.2	2.0	no
3	Lodgepole pine H24	24.7	0.4	3.4	yes
4	Lodgepole pine H19	19.3	0.5	4.0	no
5	Lodgepole pine H25	25.0	0.5	4.0	yes
6	subalpine fir H21	21.4	0.3	3.1	no
7	subalpine fir H26	26.2	0.4	3.8	no
8	Englemann spruce H23	22.9	0.2	2.4	no
9	Englemann spruce H27	27.6	0.4	3.8	yes
10	cutblocks	N/A	N/A	N/A	yes
11	regenerating cutblocks	0.6	0.01	0.5	yes

[a]Air-photo derived BC Ministry of Forests digital forest cover map for 2001.
[b]Literature values: *Jakubauskas* [1996]; *Kollenberg and O'Hara* [1999]; *Law et al.* [2001].
[c]Inventory by *Smith* [1984].

perature have been measured on an hourly basis in large forest openings at the lower elevation P1 site (1620 m) since August 1997 and at the upper elevation PB site (1900 m) since September 1999 (Figure 1a). Meteorological sensors were monitored with Campbell Scientific, Inc., CR10 data loggers. Instruments were checked through intercomparison of weather stations in 240 Creek and 241 Creek and an additional station in nearby Dennis Creek. Rain gauges were calibrated. Winter precipitation (snowfall water equivalent) was estimated using hourly snow depth measurements (Campbell Scientific, Inc., ultrasonic distance sensors) assuming a density of 100 kg/m^3.

3.2.2. Snow Water Equivalent (SWE) of the Snowpack

[15] SWE was measured at 2-week intervals starting early March at the lower elevation (1630 m) clear-cut (UPC1-CC) and mature forest (UPC1-MF) sites (using 32 points on a 105 × 45 m grid at each site) during the period 1998–2001, and during 2000–2001 at the upper elevation (1900 m) clear-cut (UPC2-CC) and mature forest (UPC2-MF) sites (Figure 1) [*Winkler*, 2001]. The UPC2-CC site may be subject to wind redistribution of snow (not accounted for in the model), and data from the site were not used.

3.2.3. Clear-Cut Snowmelt Rates

[16] Data from two snowmelt lysimeters at the P1 site provide daily measurements of meltwater outflow from the bottom of the snowpack for 1998–2001. The lysimeters consist of 2.4 × 1.2 × 0.15 m open, fiberglass-coated plywood boxes that drain to tipping bucket gauges [*Winkler*, 2001; *Spittlehouse and Winkler*, 2002].

3.2.4. Clear-Cut and Forest Snow Albedo

[17] Solar reflection from the clear-cut snowpack was measured using the upward facing LiCor pyranometer of the P1 station and a downward facing Epply pyranometer in April–May 2001 and 2002. Upward and downward facing Epply pyranometers under the canopy at P5 (vegetation class 4, Figure 1, Table 1) were used in April–May 2002 to give snow albedo of the forest snowpack. Daily average albedo was calculated for the period of noon plus and minus 4 hours. The LiCor pyranometer was checked against a calibrated Epply.

3.2.5. Below Canopy Radiation

[18] The pyranometers used for the snow albedo measurements also provided measurements of solar radiation transmittance through the canopy. Daily average transmittance was calculated for the period of noon plus and minus 4 hours. In the latter part of 2002, the pyranometers were replaced with a Kipp and Zonen CNR1 radiometer that provided measurement of upward and downward shortwave and longwave radiation. The canopy view factor V_f (equation (7b)) was estimated from measured daily incident longwave radiation below the canopy, calculated above-canopy downward longwave radiation [*Monteith and Unsworth*, 1990], and calculated longwave radiation emitted by the trees assuming they were at air temperature. Manual pyranometer transects were made in May 2003 to assess the ability of the single spot transmittance measurements to characterize the stand.

3.2.6. Rainfall Interception

[19] Rainfall interception loss was determined as the difference between above-canopy rainfall measured at the P1 weather station and the sum of throughfall and stemflow measured at the P7 site (Figure 1, vegetation class 5 in Table 1). Five 6 × 0.1 m throughfall troughs and five stemflow collectors [*Spittlehouse*, 1998] were continuously monitored during summer 1997–2001. Data were summarized on a storm basis and used to generate a relationship between interception and storm size.

3.2.7. Tree Transpiration

[20] Daily stand transpiration at the P7 site was calculated from measurements of water flow in the stems of nine trees during June–October 2000 [*Spittlehouse*, 2002]. Thermal dissipation probes in the sapwood [*Vertessey et al.*, 2001] and measured sapwood area at 1.5 m height were used to calculate daily water flow up the trunks. A relationship between tree water use and crown volume was used to scale from the tree to stand transpiration.

3.2.8. Soil Water Content

[21] Soil water content was measured from late May to October 1997–2001 in the forest at P7 and in the P1 clear-cut using time domain reflectometry (TDR) [*Spittlehouse*, 2000]. Sampling locations were randomly located along a 100 m long transect at each site.

3.2.9. Streamflow

[22] Hourly streamflow has been measured by two Water Survey of Canada (WSC) gauging stations located at the bottom of Creeks 240 and 241 since November 1983

Table 2. Constant Vegetation Parameters

Parameter	Overstory (Classes 2–9, 11)	Understory (Classes 3, 5, 9)	Origin[a]
Fractional trunk space height ( )	0.5	N/A	field estimate
LAI multiplier for rain, m	0.0012	0.0012	Figure 10
Snow interception efficiency ( )	0.7	N/A	Figure 6a
Maximum snow interception capacity, m SWE	0.02	N/A	Figure 6a
Minimum melt needed for mass release, m SWE	0.002	N/A	L1
Snow mass release/drip ratio ( )	0.4	N/A	L1
Aerodynamic attenuation coefficient ( )	3.0	N/A	L2
Albedo ( )	0.10	0.15	L2
Radiation attenuation coefficient ( )	1.7	N/A	Figure 5
Maximum stomatal resistance, s/m	5000.	5000.	L3
Minimum stomatal resistance, s/m	400.	70.	L4
Soil moisture below which transpiration is restricted ( )	0.10	0.10	Figure 11a
Vapour pressure deficit causing stomatal closure, Pa	4000.	4000.	L3
Critical light level R_{pc}, W/m^2	30.	30.	L3
Root fraction in soil layer 1; 2 ( )	0.7; 0.3	0.99; 0.01.	*Hope* [2001]
Depth of root zone layer 1; 2, m	0.3; 0.2	0.3; 0.2	*Hope* [2001]

[a]Literature values are L1, *Storck* [2000]; L2, *Campbell and Norman* [1998]; L3, *Wigmosta et al.* [1994]; L4, *Waring and Franklin* [1979] and *Wu et al.* [2000].

(Figure 1a). WSC considers streamflow measurement accuracy to be about 10%.

3.3. Model Input and Calibration

[23] DHSVM requires point information for meteorological data and spatially distributed information on terrain, vegetation, soils, stream channels, and forest roads. The preparation of this input data and subsequent stepwise model calibration followed the approach outlined by *Whitaker et al.* [2003]. For August 1997 to August 1999, hourly meteorological data were only available from the P1 site, while between September 1999 and August 2001 data from both P1 and PB were used. For the latter period, hourly temperature gradients were calculated from data for the two stations. Between August 1997 and August 1999 a constant gradient of $-2.4°C\ km^{-1}$ was used, the average for September 1999 to August 2001. A constant precipitation gradient of zero was adopted based on monthly precipitation totals for the two stations. For 240 Creek, the drainage area derived from the 30 m DEM is 4.70 km^2 (5220 pixels), while for 241 Creek it is 4.78 km^2 (5310 pixels). Overstory species composition, stand height and age, and crown closure (fractional forest cover *F*) derived from a 2001 forest cover inventory were used to develop vegetation classes (Figure 1b, Table 1). Estimates for the remaining vegetation parameters were either based on published values or were adjusted during model calibration (Table 2). Soil classes (Figure 1c, Table 3) and soil depth (Figure 1d) were determined from field mapping by *Hope* [2001]. Soil parameters for each class were derived based on textural analyses using published empirical relationships [*Rawls et al.*, 1993] or were adjusted during calibration (Table 4). Comparison with data for two dug pits at P7 (Figure 1) shows that calibrated porosity values are generally lower than the range of 0.28 m^3/m^3 (0.55–0.65 cm depth range of soil profile) to 0.74 m^3/m^3 (upper 10 cm) determined from bulk density measurements [*Spittlehouse*, 2000]. Calibrated vertical and horizontal hydraulic conductivity values are about an order of magnitude higher than laboratory values obtained on samples from the top 0.7 m of soil. This is in line with findings from tracer tests conducted in similar soils in coastal BC [*Hetherington*, 1995] which have revealed downslope flow velocities that are 1–2 orders of magnitude higher than what might be expected based on soil matrix properties. The bias between calibrated and measured porosity and conductivity values favors infiltration and

Table 3. Soil Materials and Textural Analysis

Class	Dominant Genetic Material[a]	Characteristics for Root Zone Layer 1:2				
		Texture[b]	% Sand	% Silt	% Clay	% Coarse Fragments
1	bedrock	LS/SL	72	26	2	50–90
2	morainal-colluvial-MD	SL:LS/SL	60:76	35:21	5:3	40–60:40–70
3	morainal-colluvial-VS	cSL:LS/SL	70:80	26:17	4:3	40–60:50–80
4	morainal-colluvial-S	SL:LS/SL	67:80	28:17	5:3	40–60:40–70
5	morainal-D	SL/LS/SL	60:75	35:20	5:5	40–60:40–70
6	morainal-fluvial -MD	SL:LS/SL	50:75	45:20	5:5	40–60:40–70
7	glaciofluvial-MD/D	SL:LS	55:75	40:22	5:3	35–70:40–70
8	glaciofluvial-D	SL:LS	65:75	30:22	5:3	35–70:40–70
9	fluvial-morainal-MD	SiL:SL/LS	40:55	55:40	5:5	0–10:40–70
10	fluvial-organic-MD	SiL[c]:SL/LS	40:55	55:40	5:5	0–10:20–70

[a]Description followed by depth code: VS, very shallow (0.1–1.0 m); S, shallow (1.0–2.0 m); MD, moderately deep (2.0–4.0 m); and D, deep (>4.0 m).
[b]S, sand(y), Si, silt(y), L, loam, C, clay; lowercase "c" refers to coarse.
[c]Fifteen percent organic content.

Table 4. Model Parameters for Each Soil Class and Layer

Soil Class	Soil Layer	Porosity[a]	Saturated Hydraulic Conductivity, m/s		Pore Size Distribution Index[c]	Air Bubbling Pressure,[c] m	Field Capacity[c]	Wilting Point[a]
			Vertical[a]	Lateral[a,b]				
1	1	0.10	7.0×10^{-4}	3.5×10^{-3}	0.42	0.10	0.06	0.040
2	1	0.32	8.2×10^{-4}	7.1×10^{-3}	0.37	0.10	0.20	0.045
	2	0.24	1.5×10^{-3}		0.45	0.10	0.14	0.015
3	1	0.30	1.1×10^{-3}	6.2×10^{-3}	0.40	0.09	0.18	0.025
	2	0.23	1.5×10^{-3}		0.47	0.10	0.13	0.015
4	1	0.32	9.7×10^{-4}	8.6×10^{-3}	0.38	0.09	0.19	0.035
	2	0.23	1.9×10^{-3}		0.47	0.10	0.13	0.045
5	1	0.32	8.2×10^{-4}	6.2×10^{-3}	0.37	0.10	0.20	0.045
	2	0.24	1.2×10^{-3}		0.44	0.10	0.15	0.025
6	1	0.33	5.8×10^{-4}	6.1×10^{-3}	0.35	0.12	0.25	0.055
	2	0.24	1.2×10^{-3}		0.36	0.10	0.16	0.015
7	1	0.33	7.0×10^{-4}	7.1×10^{-3}	0.48	0.11	0.21	0.050
	2	0.24	1.5×10^{-3}		0.45	0.11	0.16	0.015
8	1	0.32	8.8×10^{-4}	7.2×10^{-3}	0.38	0.09	0.20	0.040
	2	0.24	1.5×10^{-3}		0.45	0.11	0.16	0.015
9	1	0.35	8.8×10^{-4}	3.3×10^{-3}	0.35	0.14	0.21	0.070
	2	0.27	6.3×10^{-4}		0.39	0.15	0.16	0.050
10	1	0.29	8.8×10^{-4}	4.0×10^{-3}	0.37	0.18	0.18	0.070
	2	0.27	7.7×10^{-4}		0.39	0.15	0.14	0.050

[a]Figure 13c: Parameters were adjusted uniformly across soil classes/layers using shuffled complex evolution algorithm by linking DHSVM with NLFIT software of *Kuczera* [1994]. Parameters were optimized for scheme 1 (Table 6).
[b]Exponential decay coefficient for saturated lateral hydraulic conductivity is equal to 4.5 for all soil classes.
[c]Empirical relationships of *Rawls et al.* [1993].

runoff over changes in soil water storage and may reflect a need for the model to account for bypass infiltration and preferential hillslope runoff. Unless indicated otherwise, calibrated model parameters (Table 2, Table 4) were derived from measurements for water year 1999, which was chosen based on completeness of the 240 Creek streamflow record. SWE and streamflow data for the other 3 years were held back for model performance evaluation. The 241 Creek hydrograph was also not used during calibration but was used to assess the transferability of model parameters between the two basins.

4. Results

4.1. Clear-Cut Snow Albedo and Snowmelt

[24] Energy balance measurements (net radiation, soil heat flux, sensible heat flux, and latent heat flux) at Mayson Lake (51°13′N, 120°29′W) 150 km north of UPC have shown that except under strong winds, sensible and latent heat fluxes to a clear-cut snowpack are small compared with radiation fluxes under south central BC conditions [*Adams et al.*, 1998]. Eddy fluxes were small due to the stability of the atmosphere resulting from the strong lapse in temperature above the cold pack. Most of the energy available for melt resulted from shortwave radiation. On the basis of these Mayson Lake findings, the emphasis at UPC was put on snow albedo controlling the amount of shortwave radiation absorbed at the snow surface and melt of the clear-cut snowpack.

[25] The ability of the albedo decay functions (equation (4)) to represent temporal snow reflectivity variations was evaluated using spring 2001 clear-cut albedo measurements for the P1 site. Model-predicted hourly snow albedo was averaged over the 0800–1600 LT period to obtain daily-average values consistent with the measurements. Between 11 April and 13 May, variations in snow albedo result from the duration each day that the snowpack is under freezing ($T_s < 0$) or melt ($T_s = 0$) conditions. The UPC-CC albedo curves (Figure 2, Table 5) provide a good overall match to this variability in snow albedo (Figure 3a). However, individual snowfall events can result in significant departures from the adopted albedo decay functions, and this is seen between 13 and 15 May. Several light snowfall events occurred during this period that result in model-predicted albedo values that are significantly higher than the measured values. Following a snowfall event, the age of the snowpack is reset to zero in the model and snow albedo assumes its initial maximum value. In reality, there is a rapid return from the high albedo of the fresh snow to the low reflectance of the old melting pack, and hence under

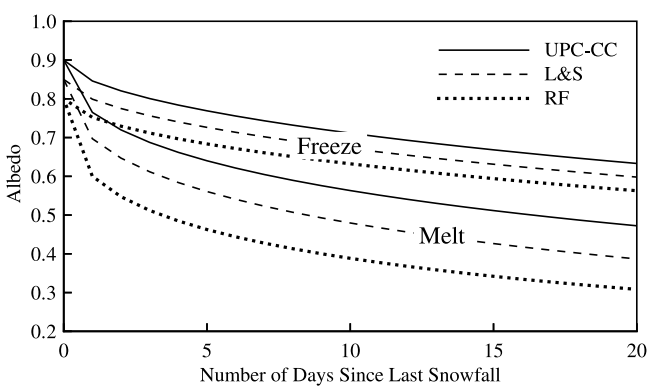

Figure 2. Albedo decay functions listed in Table 5. The UPC-CC curves are discussed in section 4.1. The Redfish Creek (RF) curves were used by *Whitaker et al.* [2003]. The *Laramie and Schaake* [1972] functions (L&S) are only shown for reference.

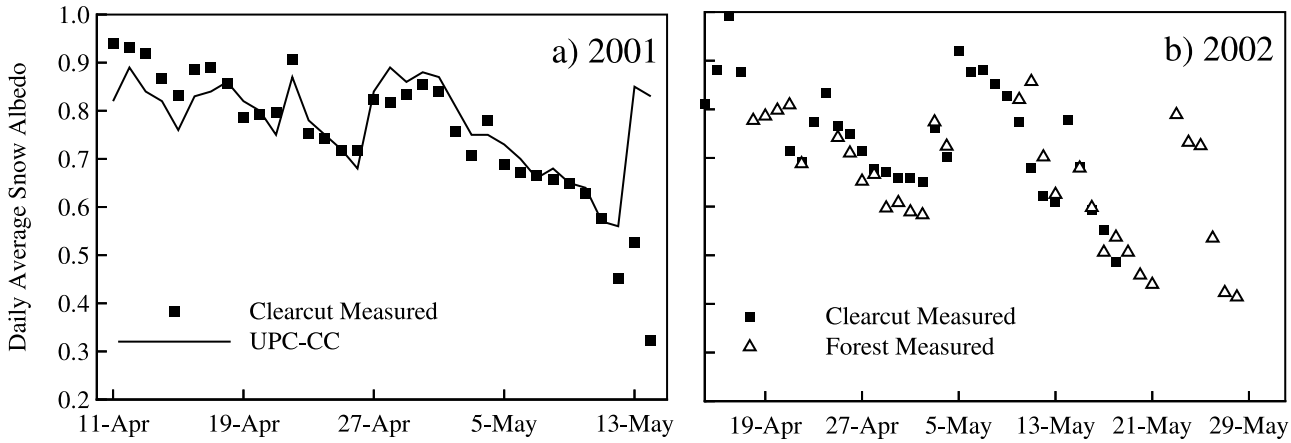

Figure 3. (a) Measured and model-predicted spring 2001 snow albedo at P1 for UPC-CC decay functions (Figure 2). (b) Measured spring 2002 snow albedo for P1 and P5. Snowfall on 21–22 May occurred when snow in the clear-cut had already disappeared.

these conditions the adopted albedo curves tend to overestimate snow reflectance.

[26] Snowmelt rates predicted using the UPC-CC albedo curves generally provide a reasonable match to the lysimeter meltwater outflow measurements (Figure 4), except for 1998 when snowmelt rates are overestimated throughout the melt season though the model does follow the trend in measured values. The 1998 melt season was characterized by an exceptionally warm spring following a sharp rise in temperature that began on 12 April, causing the entire UPC1-CC snowpack to melt away over a period of only 4 weeks compared with the usual 6 weeks. It may be that the UPC-CC albedo curve does not adequately describe snow albedo in 1998 as well as it does for other years. Except for 1998, snowmelt appears to cease while the UPC-CC model still predicts melt to occur. This is because late in the melt season, it is difficult to distinguish between rainfall and snowmelt in the lysimeter outflow. Hence lysimeter data cannot be used at this time. Several small snowmelt events are simulated at the start of the melt season when none are observed. The UPC-CC albedo curves may lead to an overestimation of early spring snowmelt, given that these curves are based on measurements for the late spring period when albedo will tend to be lower due to snowpack ripening, consequently underestimating albedo for early spring. It could also be that the lysimeters have difficulty recording the initial meltwater release. Overall, the UPC-CC albedo curves derived from measurements in spring 2001 result in snowmelt rates that are in general agreement with observed melt rates for the period 1998–2001. This establishes that the UPC-CC curves may be considered representative of albedo decay for snow in open areas.

4.2. Forest Radiation Balance and Snowmelt

[27] Energy balance measurements at Mayson Lake indicated that snowmelt below a mature forest canopy was generally dominated by net radiation [*Adams et al.*, 1998]. Eddy fluxes were reduced compared with those in the clear-cut due to low turbulent exchange down through the canopy, with wind speeds generally being only 10–20% of those in the open and below the stall speed of standard anemometers (0.5 m/s). On the basis of Mayson Lake findings, the emphasis at UPC was put on the below-canopy radiation balance and melt of the forest snowpack.

[28] At P5, point measured canopy shortwave transmittance varied from about 0.24 in the spring to 0.28 during the summer, reflecting the higher solar angle at this time, and declined again to a value of 0.18 mid-September (Figure 5). A 64-point transect of moosehorn measurements gave $F = 0.4 \pm 0.2$ [*Winkler*, 2001] while air-photo-derived crown closure for vegetation class 4 is 0.5 (Table 1). Considering the potential error in crown closure, the single-point measured range of transmissivity values is in agreement with *Reifsnyder and Lull* [1965]. The relatively uniform canopy at P5 has a base that is 10–15 m above ground, gaps in the canopy of 1–3 m in diameter, and a fairly even spacing between trees of 1–4 m. Careful placing of sensors can result in single-point transmittance estimates that are close to those obtained from multiple sensors, and this was confirmed by limited manual transect measurements for May 2003. P5 transmittance estimates are also consistent with measurements for a 20 m transect using a trolley

Table 5. Model Snow Properties

Property	Value	Origin[a]
Surface roughness length, m	0.004	L1
Water holding capacity, %	1.0	L1
UPC-CC albedo parameters	$\alpha_o = 0.90$; $A_a = 0.94$; $B_a = 0.58$; $A_m = 0.85$; $B_m = 0.46$	Figure 3a
L&S albedo parameters	$\alpha_o = 0.85$; $A_a = 0.94$; $B_a = 0.58$; $A_m = 0.82$; $B_m = 0.46$	L2
RF albedo parameters	$\alpha_o = 0.80$; $A_a = 0.94$; $B_a = 0.58$; $A_m = 0.75$; $B_m = 0.40$	L3

[a]Literature values are L1, *Spittlehouse and Winkler* [2002]; L2, *Laramie and Schaake* [1972]; and L3, *Whitaker et al.* [2003] Redfish Creek (RF) study.

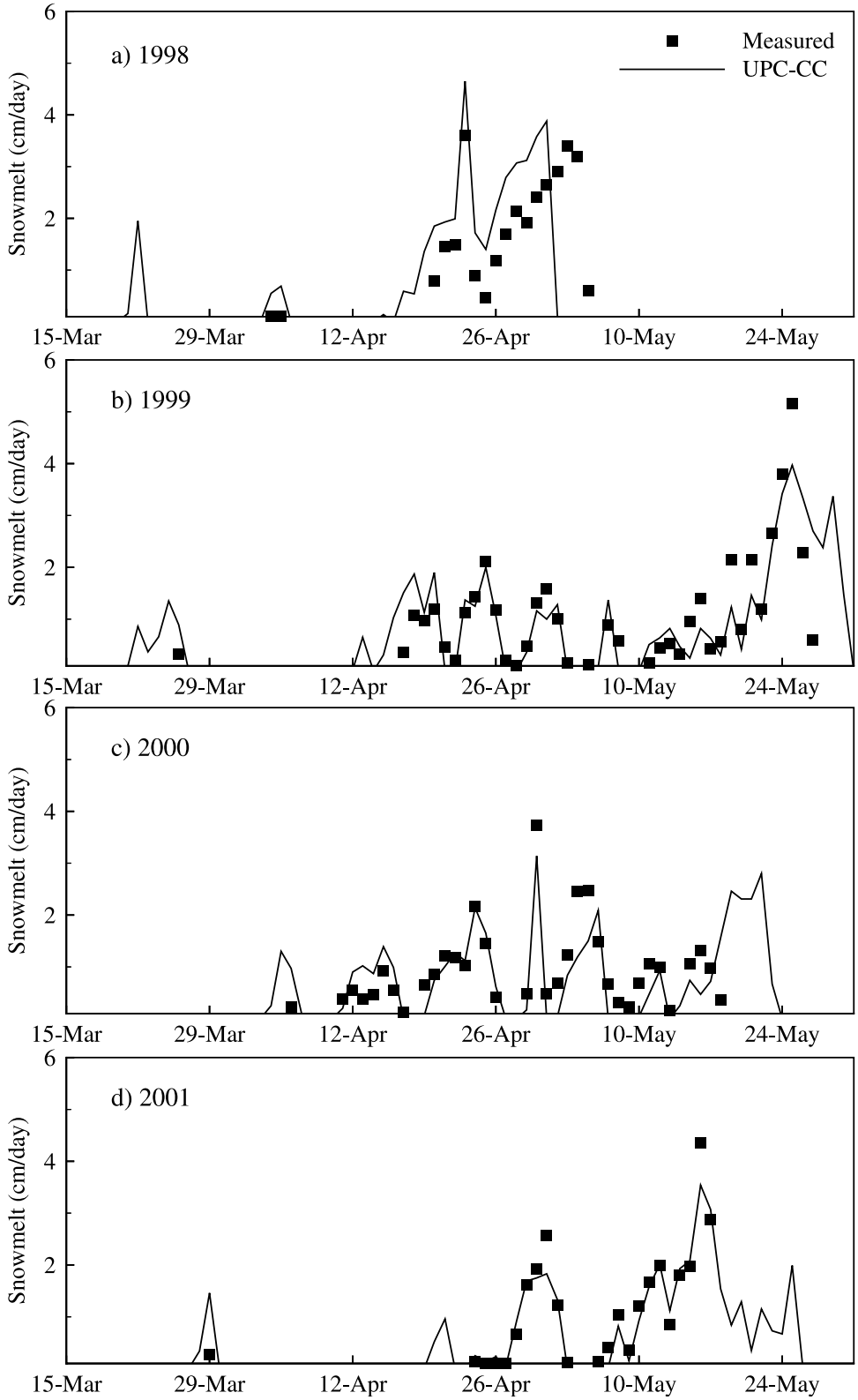

Figure 4. Measured daily lysimeter meltwater outflow at P1 clear-cut site and model-predicted snowmelt for UPC-CC albedo functions (Figure 2).

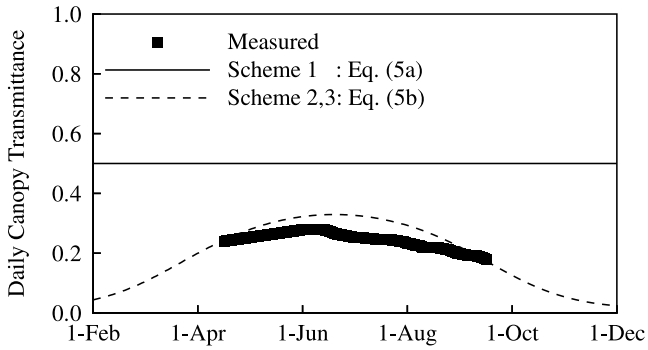

Figure 5. Comparison of measured daily average below-canopy transmittance at P5 site for 2002 with simulated transmittance for three forest radiation balance schemes (Table 6). Schemes 2 and 3 produce identical results.

system at Mayson Lake [*Adams et al.*, 1998], where it was found that in April about 18% of incident solar radiation was transmitted through a canopy of 23 m tall Englemann spruce, subalpine fir, and lodgepole pine with $F = 0.54$.

[29] DHSVM's approach for calculating pixel-average canopy shortwave attenuation (equation (5a)) is inconsistent with P5 transmittance estimates. Even with k_{LAI} set to a large value yielding $\tau_i = 0$, the minimum possible value for a forest stand with $F = 0.5$ is $\tau_c = 0.5$ (Figure 5). The variability in crown closure of ±0.2 is insufficient to explain the discrepancy between measured and simulated shortwave transmittance. The alternative formulation (equation (5b)) for attenuating shortwave radiation was therefore incorporated in the model and a value $K_F = 1.7$ was adopted to match measured daily shortwave transmittance for April 2002 at P5, this being the best estimate available at the time. Model-predicted hourly transmittance was averaged over the 0800–1600 LT period to obtain daily-average values consistent with the measurements. The simulated pattern of change in canopy shortwave transmittance over the period of measurement is somewhat stronger than measured but within the accuracy of the data.

[30] Calculations based on the P5 daily longwave measurements (14 observations) suggest that $V_f = 0.81 \pm 0.07$. Despite uncertainty in the calculation of above-canopy longwave radiation and the small differences between the various longwave fluxes, it is clear that DHSVM's approach for determining longwave radiation fluxes (equation (7a)), suggesting $V_f = F = 0.5 \pm 0.2$, is inconsistent with the estimated view factor. The fact that DHSVM's formulation for calculating the forest radiation balance (scheme 1, Table 6) overestimates canopy shortwave transmittance (Figure 5) and underestimates longwave radiation emitted by the forest canopy ($F < V_f$) but can still reproduce the measured rate of decline of melt-period forest SWE (Figure 6) underscores the value of the P5 radiation measurements in constraining shortwave and longwave contributions to net radiation fluxes to the forest snowpack.

[31] Surface litter and protruding understory vegetation can result in the forest albedo being lower than that in the open. At P5, the understory is less than 0.2 m tall and does not protrude above the pack, the situation in much of the watershed. Measured albedo for spring 2002 is similar to that of the clear-cut (Figure 3b), suggesting that litter produced by the lodgepole pine forest had a limited effect on snow albedo. These conditions are represented in scheme 2 (Table 6), in which $V_f = 0.85$ ($1.7 \times F$) results in simulated snowmelt rates that match melt period SWE (Figure 6) and net radiation fluxes to the forest snowpack that are similar as in scheme 1 (Figure 7). However, in scheme 2 longwave radiation is more important for snowmelt and shortwave radiation is less important than in scheme 1. An alternative hypothesis was allowed for, in which P5 forest snow albedo measurements (Figure 3b) are discounted as not representative for the entire catchment and where melt period snow albedo in the forest is taken to be lower than that in clear-cuts. This hypothesis is represented in scheme 3 (Table 6), in which the RF albedo curves (Figure 2, Table 5) used in the Redfish Creek (RF) study of *Whitaker et al.* [2003] were adopted for forested areas ($F > 0$). In this case $V_f = 0.7$ ($1.4 \times F$) matches observed melt period SWE at UPC1-MF (Figure 6). Scheme 3 is intermediate between scheme 1 and 2 in terms of the relative importance of longwave and shortwave contributions to net radiation (Figure 7). Scheme 3 illustrates that even if forest snow albedo is in fact lower than that in the clear-cut, as some of the literature suggests [*Barry et al.*, 1990; *Hardy et al.*, 1997, 2000], the view factor required to match melt-period SWE is still in agreement with the radiation data. This emphasizes the need for the revised forest radiation balance.

4.3. Snow Accumulation and Melt at UPC1

[32] Snow accumulation and melt patterns at the UPC1-CC and UPC1-MF sites for 1998–2001 (Figure 8) were used to assess the model's ability to simulate the impact of clear-cut logging on snow processes in the context of weather variability. In 1998, characterized by a fast spring temperature rise and resultant rapid snowmelt rates, the snowpack is predicted to disappear a little earlier than observed. This is a consequence of the overestimation of snowmelt rates for this year by the model (Figure 4a). In the remaining years 1999–2001, simulated SWE is in excellent agreement with the measurements in both clear-cut and forest. This demonstrates that the model is able to reproduce year-to-year variability in measured differences in snow accumulation and melt between the UPC1-CC and UPC1-MF sites. Differences in measured peak SWE between forest and clear-cut illustrate that the net snow interception

Table 6. Forest Radiation Schemes Considered

	Scheme 1	Scheme 2	Scheme 3
Shortwave radiation	equation (5a); $k_{\mathrm{LAI}} = \propto$	equation (5b); $k_F = 1.7$	equation (5b); $k_F = 1.7$
Longwave radiation	equation (7a)	equation (7b); $V_f = 1.7F$	equation (7b); $V_f = 1.4F$
Clear-cut albedo ($F = 0$)	UPC-CC	UPC-CC	UPC-CC
Forest albedo ($F > 0$)	UPC-CC	UPC-CC	RF

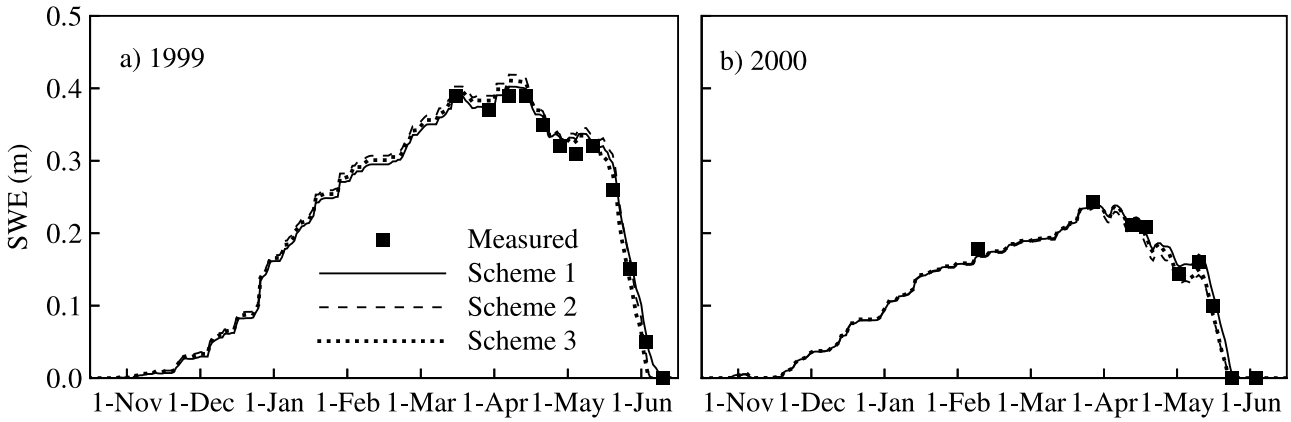

Figure 6. Measured and model-predicted SWE at UPC1-MF forest site for three forest radiation balance schemes (Table 6).

efficiency of the canopy over an entire accumulation season is much less than $f = 0.7$ (Table 2), and is instead of the order of 10–30%, as correctly simulated by the model. This suggests that during snowfall events the canopy is often close to its interception capacity, such that interception is much smaller than predicted by equation (1). The performance of schemes 2 and 3 in simulating snowmelt in the forest is very similar for each of the 4 years of simulation.

4.4. Snow Accumulation and Melt at UPC2-MF

[33] SWE measurements for UPC2-MF (Figure 9) were used to further evaluate model-predicted forest snowmelt, based on elevation differences between this site and UPC1-MF (1900 m versus 1650 m). Both UPC1-MF and UPC2-MF are characterized by a southerly aspect (Figure 1a) and receive similar shortwave radiation inputs. Because of lower air temperature at higher elevation, longwave radiation fluxes are smaller at UPC2-MF than at UPC1-MF. As a result, the onset of snowmelt and the timing of snowpack disappearance are somewhat delayed for UPC2-MF relative to UPC1-MF in 2000 (compare Figure 8c and Figure 9a). These patterns are well reproduced by the model. Because of the absence of SWE measurements late in the melt season, it is not possible to assess the model performance in this respect for 2001. Again, the performance of schemes 2 and 3 in reproducing measured forest SWE is very similar despite differences in longwave radiation inputs between the UPC2-MF and UPC1-MF sites and despite differences in the relative importance of shortwave and longwave radiation for model-predicted snowmelt rates between the two schemes. The results for 2000 suggest that both forest radiation schemes are able to reasonably reproduce changes in forest snowmelt due to changes in elevation.

4.5. Rain Interception

[34] At UPC, rainfall accounts for 30–50% of annual precipitation. Consequently, evaporation of intercepted rain is an important component of the annual evaporation budget and rain interception will also affect soil moisture levels in the forest. Model-predicted canopy rainfall interception was compared with interception measurements (rainfall minus throughfall and stemflow) at the P7 site for summer 1997 and 1998. Stemflow is not considered in the model but measured stemflow was small, reaching a maximum of only 2% of rainfall size for events greater than 20 mm. Following *Spittlehouse* [1998], individual rainfall events are defined in the analysis below as being separated by at least 2 hours without precipitation. Measured and model-predicted throughfall exhibit substantial scatter between individual rainfall events due to the importance of antecedent conditions, and only trends in throughfall versus event size were evaluated.

[35] With R_m set to 1.2 mm (Table 2), the rain interception capacity of the forest stand at P7 (vegetation class 2; Table 1) is $F \times \mathrm{LAI} \times R_m = 2.4$ mm in the model. Total interception during a rainfall event may exceed this value due to evaporation from wet vegetation surfaces. Model-predicted throughfall for June–September 1997 and 1998 was plotted versus event size and compared with the *Spittlehouse* [1998] data analysis (Figure 10). Model-predicted rainfall interception is about 50% of rainfall for small events until it reaches a maximum of about 2.8 mm, as defined by separate linear trend lines fitted to simulated throughfall for events smaller and greater than 8 mm. These fitted trend lines are in general agreement with actual rainfall interception losses, defined by Spittlehouse as $I = 3.9(1 - \exp(-0.1R))$, where R is storm size. The importance of antecedent conditions is illustrated by two consecutive storms on 16–17 September 1997. The model predicts interception losses for the first 6.2 mm storm to be 2.7 mm, filling much of the storage capacity of the canopy, while for the second 29 mm storm only 1.3 mm of interception losses are predicted. In comparison, Spittlehouse measured these interception losses to be 2.3 and 1.4 mm, respectively.

4.6. Soil Moisture and Evaporation

[36] Soil moisture data collected in the forest near P7 for summer 1998 and 1999 were used to evaluate the model performance in simulating evaporation. The summer of 1998 was quite dry, whereas 1999 was much wetter with frequent rainstorms, and this is reflected in the water content data for the upper (0–0.3 m) and lower (0.3–0.5 m) root zone (Figure 11). The model is able to reproduce the gradual decline in 1998 soil moisture in both root zones, with the greatest drying taking place in the upper 0.3 m of the soil. The rapid soil moisture fluctuations in 1999 in the upper root zone are more difficult to predict but are still reasonably represented by the model. On the other hand, simulated

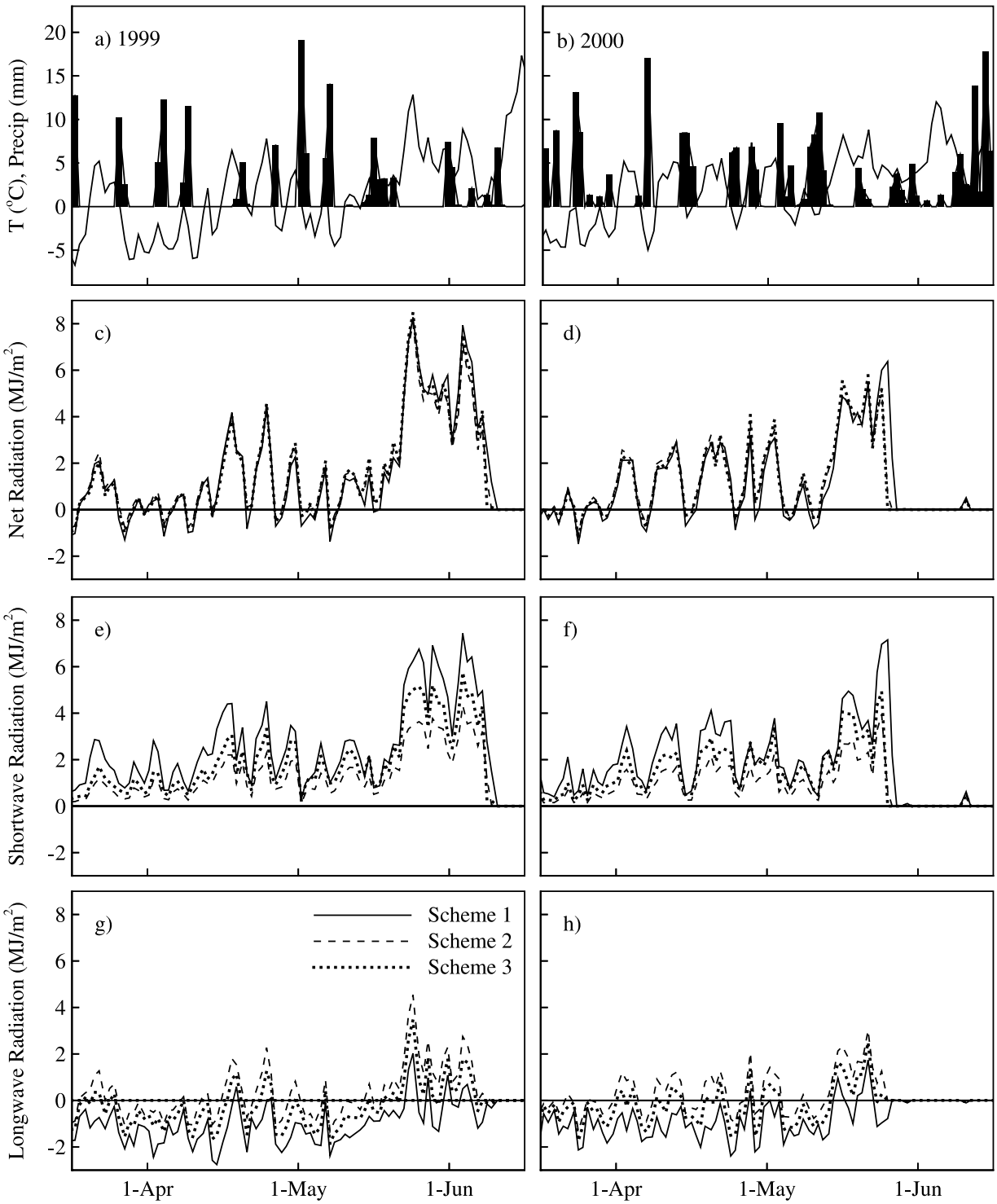

Figure 7. Temperature and precipitation at P1 (Figures 7a and 7b) for 1999 (left) and 2000 (right) together with computed daily radiation exchanges at UPC1-MF snow surface (Figures 7c and 7d), shortwave (equation (3)) contributions (Figures 7e and 7f), and longwave (equation (7)) contributions (Figures 7g and 7h).

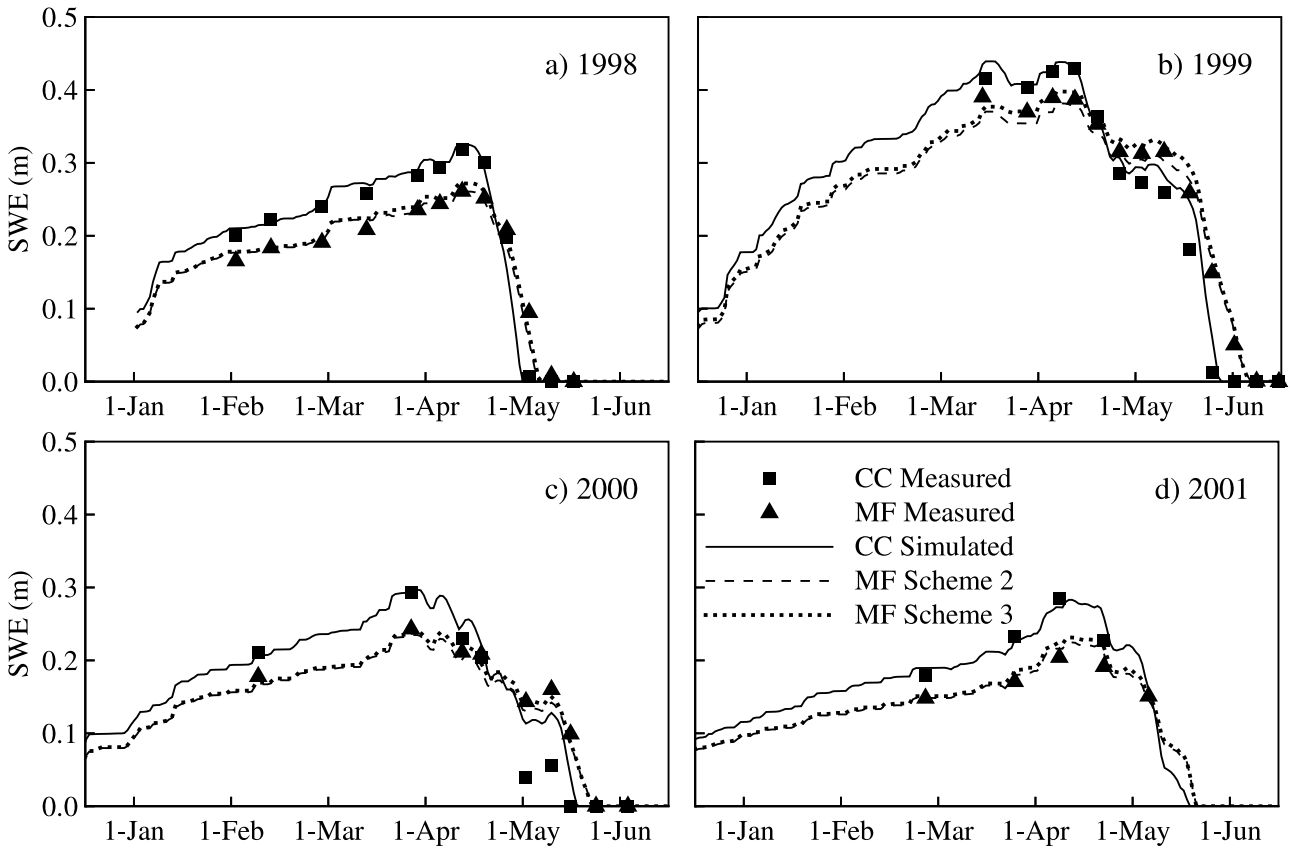

Figure 8. Measured and model-predicted SWE at UPC1-CC clear-cut site and UPC1-MF forest site for schemes 2 and 3. Clear-cut simulations (CC-simulated) are identical for both schemes.

lower root zone soil moisture for 1999 exhibits more fluctuations and is on average higher than observed.

[37] The model's capture of the different response of soil moisture to dry and wet summers suggests that total evaporation due to transpiration by overstory (trees) and understory (shrubs, herbs) and soil evaporation is well simulated. Variations in daily tree transpiration rates derived from 19–24 July 2000 sap flow measurements in the P7 forest are also reproduced by the model (Figure 12). Model-predicted daily tree transpiration for most dry days is within 10% of the measured values but for 22–23 July, characterized by overnight rainfall, tree transpiration is underpredicted by 19% and 31%, respectively. This suggests that evaporation rates for intercepted rain are perhaps underestimated in the model, causing intercepted water to remain in the canopy too long and limiting tree transpiration. Overall, this assessment suggests that the model yields reasonable forest evaporation rates.

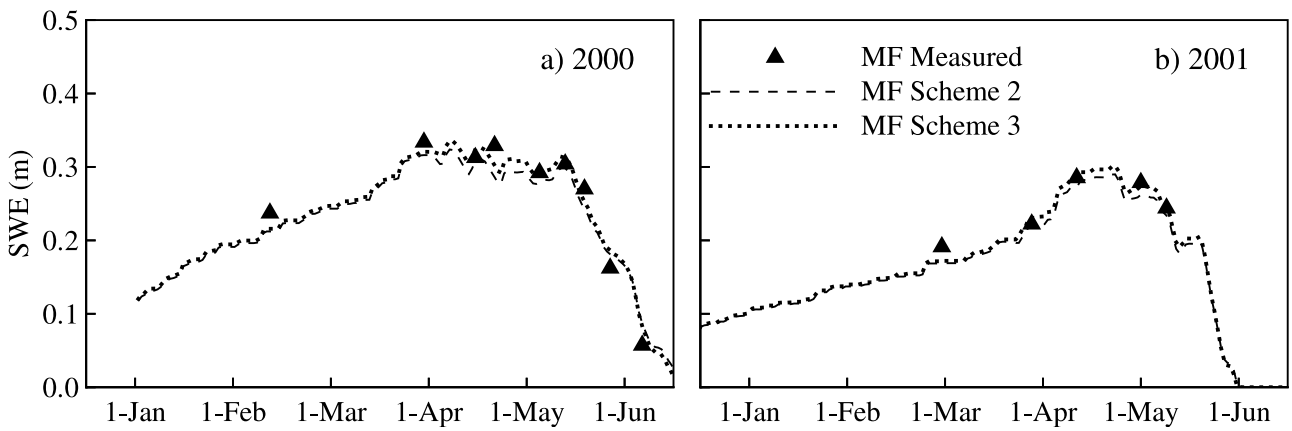

Figure 9. Measured and model-predicted SWE at UPC2-MF forest site for schemes 2 and 3.

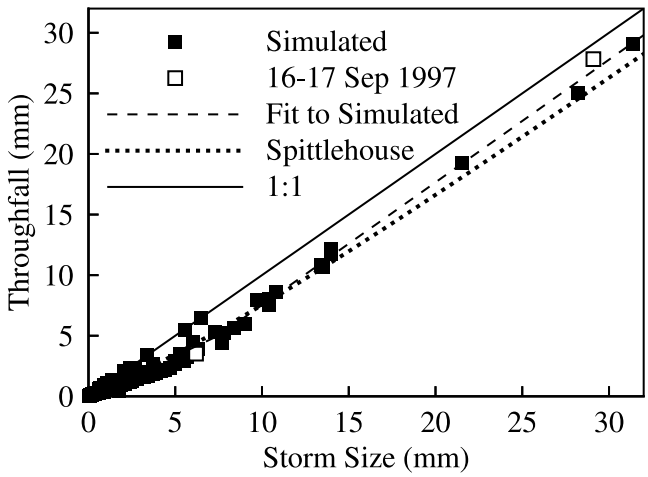

Figure 10. Model-predicted throughfall versus event size at P7 together with exponential trend line determined from *Spittlehouse* [1998] throughfall data. The 16–17 September 1997 events were analyzed in detail as discussed in text.

[38] Unfortunately, data collected in the P1 clear-cut cannot be used directly in the model assessment as this clear-cut is located outside of the drainage area for the two catchments (Figure 1a). However, from his analysis of P1 and P7 soil moisture data, *Spittlehouse* [2000] concluded that forest and clear-cut evaporation rates discounted for rain interception appear to be very similar. In comparison, for the October 1999 to September 2001 simulation period (following logging at UPC2-CC), total evaporation discounted for rain interception is 321 mm for P7 and 380 mm for UPC2-CC. The model therefore suggests that evaporation in the UPC2 clear-cut is about 18% higher than in the P7 forest. Similarity of forest and clear-cut evaporation rates may seem surprising, but it is consistent with other studies [*Adams et al.*, 1991; *Vertessey et al.*, 2001].

4.7. Streamflow for 240 Creek

[39] Streamflow simulations were used to assess differences in model performance when alternative conceptualizations of the radiation balance are extrapolated across forest stands with different physical characteristics (Table 1). A fixed linear relationship was assumed between the canopy view factor V_f and fractional forest cover F, as determined for vegetation class 4 at UPC1-MF (Table 6). This is a simplifying assumption, as this relationship may be expected to vary depending on crown closure, tree height, and species composition. Identical soil parameters, obtained for scheme 1, were used in assessing differences in simulated streamflow. Three separate performance measures were used for model testing: volume error $\delta V/V$ between simulated and observed flows, model efficiency $E!$ [*Nash and Sutcliffe*, 1970] relating how well calculated and observed flows compare in both volume and shape, and the coefficient of determination $D!$ which depends on timing of flows, but not on volume. $D!$ and $E!$ were calculated at the hourly model time step. Simulated and measured annual maximum flows are also compared: $\delta P/P$. For a sucessful model performance, $\delta V/V$ and $\delta P/P$ should be close to zero while $E!$ and $D!$ should be close to unity. *James and Burges* [1982] found that for daily flows, a coefficient of efficiency greater than about 0.97 was associated with relatively well calibrated continuous simulation models, but this value is not commonly achieved and smaller time increments will also result in a poorer $E!$ [*Gan and Burges*, 1990a, 1990b]. Summary statistics do not illustrate the strengths and weaknesses of simulated streamflow responses as completely as residual time series plots [*Burges*, 2003], and the model performance was also evaluated visually.

[40] In comparing $E!$, $D!$, and δV, it is clear that schemes 2 and 3 perform better than scheme 1 in reproducing the 240 Creek hydrograph for each of the 4 years of simulation (Table 7). Furthermore, while for scheme 1 the $E!$ and δV statistics in particular exhibit substantial year-to-year variation, these model performance statistics vary much less between years for schemes 2 and 3, indicating a more consistent model performance in the context of weather variability. The performance of the three schemes in simulating 1999 streamflow (used in calibration) is similar. Melt of the comparatively large 1999 snowpack (Figure 6) and the resulting hydrograph rise occurred later than in other years (Figure 13). In contrast, 1998 and 2001, both characterized by an early hydrograph rise, have the greatest differences in performance statistics (Table 7). Schemes 2 and 3 perform about equally well in reproducing the 240 Creek hydrograph for the 4-year period (Figure 13, Table 7).

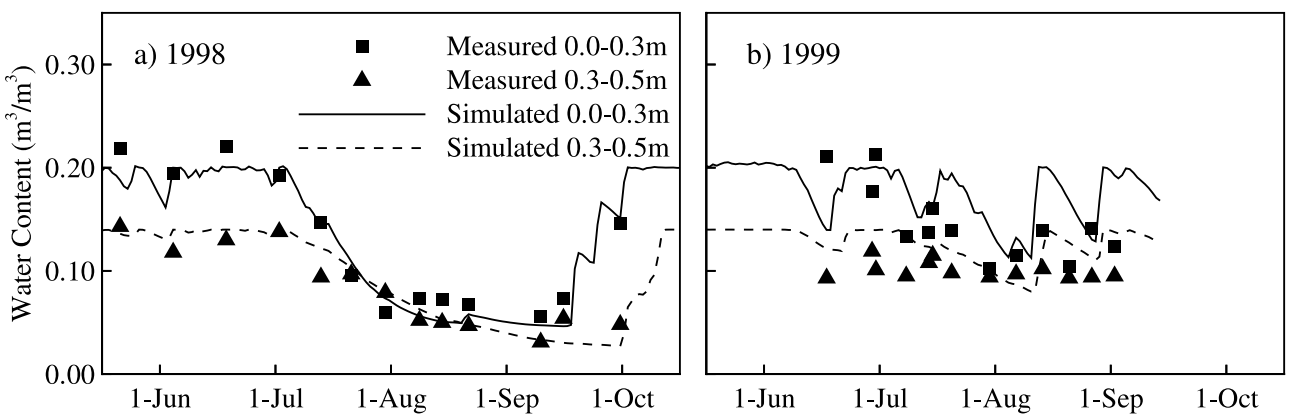

Figure 11. Measured and model-predicted soil water content in two root zone layers at P7 site for scheme 2. Results for scheme 3 are virtually identical to those for scheme 2.

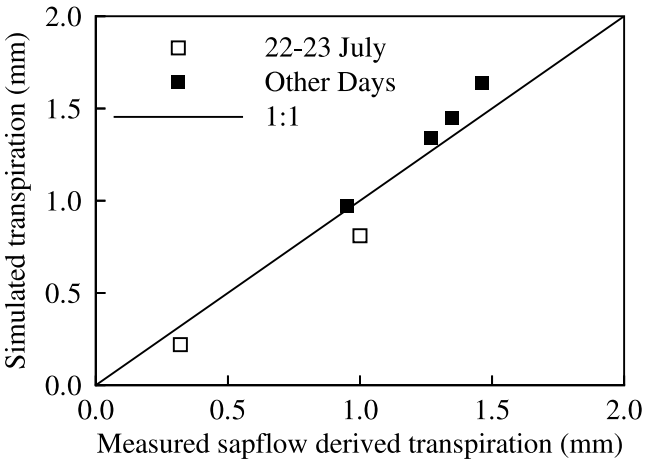

Figure 12. Comparison of daily tree transpiration determined from 19–24 July 2000 sap flow measurements at P7 site with model-predicted daily overstory transpiration. Results for schemes 2 and 3 are identical. Rain fell overnight on 22–23 July.

Differences between these two schemes are only apparent when comparing simulated and measured peak flows. Scheme 3 performs better in reproducing annual maximum flows while scheme 2 has a tendency to underestimate peaks for 240 Creek. The 4-year average values for *E!* of 0.90 (scheme 2) and 0.91 (scheme 3) are considerably closer to the target value of 0.97 for a well-calibrated model than the 0.84 value for scheme 1, considering that model efficiency was calculated at an hourly time step. Residual time series plots (Figure 13) indicate where model improvements are still required, but no general trend is apparent. In 1998, measured streamflow is overestimated by the model at the start of the melt season and falls off too quickly. Conversely, in 1999, 2000, and 2001, the simulated rising limb of the hydrograph starts somewhat later than measured while the recession limb tends to fall off a bit too slow.

[41] Performance statistics for the three radiation balance schemes for 2000 are typical of the 4-year average (Table 7), and this water year was used to examine the cause of differences in streamflow simulation. Simulation results suggest that these differences are derived from dissimilarities in snowmelt, while evaporation is dominated by intercepted rainfall evaporation and tree transpiration and therefore virtually unaffected by the conceptualization of below-canopy radiation (Figure 14). Schemes 2 and 3 are characterized by greater early-season melt than scheme 1 and lower basin-aggregated melt later in spring when the snowpack starts disappearing. The signature of these seasonal differences in snowmelt is subtly visible in UPC1-MF SWE simulations for 2000 but not in 1999 (Figure 6). In 2000, most snowmelt occurred from mid-April to mid-May at a time when shortwave fluxes were relatively low (Figure 7f), resulting in somewhat higher net radiation fluxes to the forest snowpack for schemes 2 and 3 as compared with scheme 1 (Figure 7d). In contrast, most 1999 snowmelt occurred mid-May to early-June at a time when shortwave radiation fluxes were higher (Figure 7e), leading to similar net radiation contributions to snowmelt for all three schemes (Figure 7c). Hence the subtle improvement in streamflow simulation appears to be derived from greater early season snowmelt for schemes 2 and 3 due to the increased importance of longwave radiation in the modified radiation balance.

4.8. Streamflow for 241 Creek

[42] Recorded 241 Creek streamflow was not used during model calibration but was used to assess whether the model is able to reproduce differences in streamflow characteristics between the two catchments without parameter adjustment (Figure 15). For simulating water year 1998 the UPC2 clear-cut that was logged in winter 1998–1999 (Figure 1b) was changed to represent prelogging conditions by filling it in with surrounding vegetation types. The catchments were winter logged, so ground disturbance is minimal. Even if soil conditions may have been altered somewhat, experience has shown that streamflow simulations at UPC are far more sensitive to snowmelt characteristics (e.g., as affected by snow albedo) than to soil properties, and hence the issue of compaction of surface soil layers was not pursued.

[43] Although *E!* and *D!* values for 241 Creek are slightly lower than for 240 Creek, most notably in 1998 and 2000 (Table 7), the model performs well in reproducing subtle differences in the hydrographs for the two catchments. Several small peaks in the 241 Creek hydrograph that occurred between late April and early May in both 1999 and 2000 and which are not as pronounced in the 240 Creek hydrograph are well simulated (compare Figures 13b and 13c to Figures 15b and 15c). These differences in early season streamflow are likely due to a combination of the higher stream network density for 241 Creek and differences in aspect between the two catchments (Figure 1a). Approximately 60% of 240 Creek is characterized by an east-southeast aspect, while 60% of the 241 Creek faces south-southwest. The slightly more southerly aspect of 241 Creek results in earlier snowmelt, as illustrated by the higher streamflow at the start of the melt season. The above comparison illustrates that DHSVM is able to capture hydrograph sensitivity to differences in physical characteristics of the two catchments.

5. Summary and Conclusions

[44] An application of the distributed hydrology soil vegetation model (DHSVM) was developed for the 240 and 241 Creek paired catchments, part of the Upper Penticton Creek (UPC) Watershed Experiment in south central British Columbia. This study was undertaken to investigate the ability of the DHSVM to simulate the hydrologic effects of forestry activities in the high-elevation plateau-type catchments that are typical of this region. The performance and internal structure of the DHSVM was diagnosed using 1998–2001 data, including snow water equivalent (SWE) in two clear-cuts and adjacent forest stands, clear-cut and forest snow albedo, daily snowmelt lysimeter data, below-canopy radiation, rainfall interception, tree transpiration, soil moisture, and streamflow for 240 Creek and 241 Creek.

[45] It was shown that clear-cut snowmelt rates calculated using data-derived snow albedo curves are in agreement with observed lysimeter outflow. Radiation measurements in a forest stand with air crown closure $F = 0.50$ suggest that the fraction of shortwave radiation transmitted through the

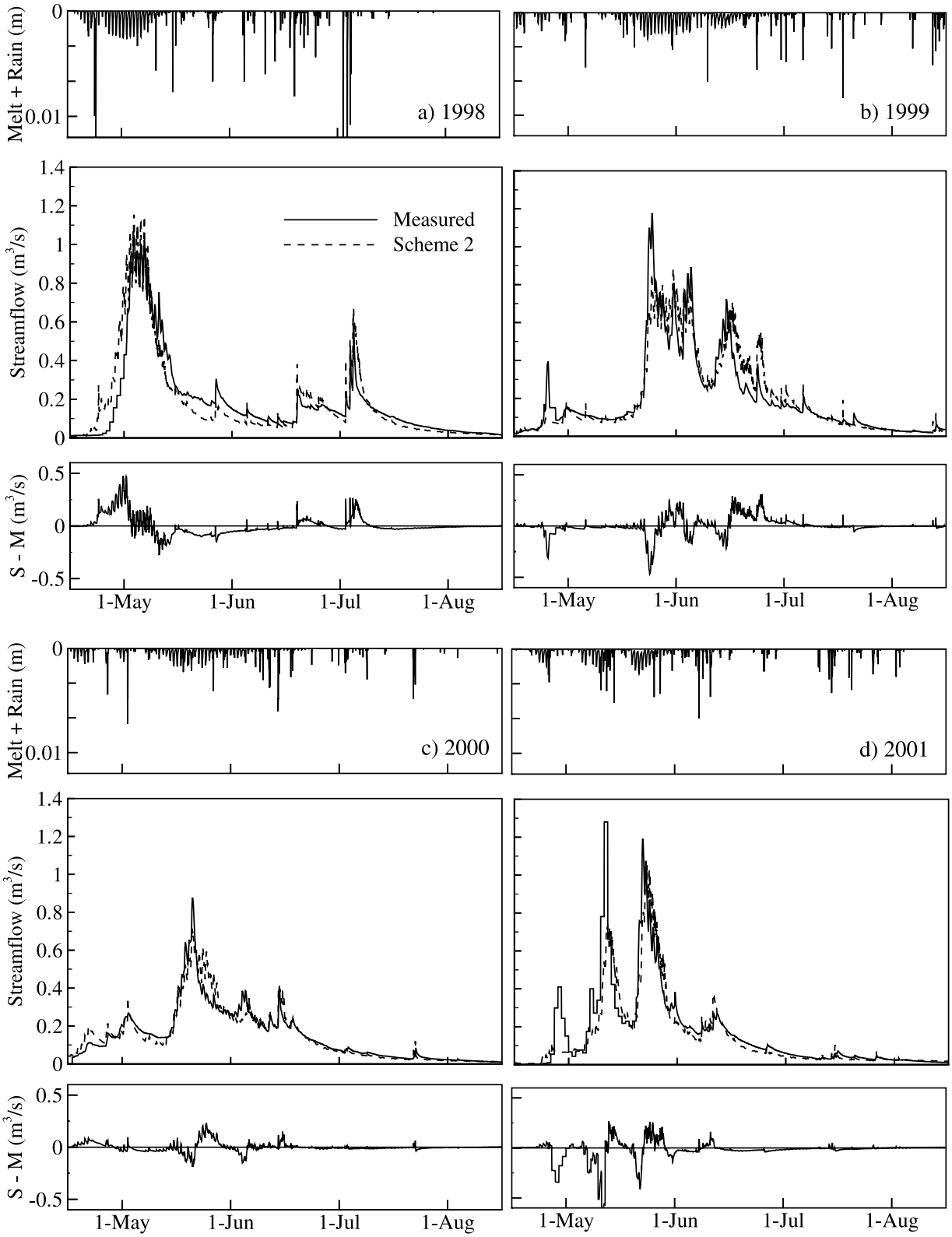

Figure 13. Measured (M) and scheme 2 simulated (S) streamflow for 240 Creek, together with residual time series S-M and simulated basin-aggregated snowmelt plus rainfall at hourly model time step. Results for scheme 3 are very similar. For early 1998 (prior to 1 May) and 2001 (prior to 21 May) only daily-average flows were available.

Table 7. Model Performance Statistics for 240 and 241 Catchments[a]

	240			241	
	Scheme 1	Scheme 2	Scheme 3	Scheme 2	Scheme 3
			1998		
E!	0.77[b]	0.86[b]	0.84[b]	0.83	0.82
D!	0.85[b]	0.88[b]	0.88[b]	0.92	0.92
δV	−0.10[c]	−0.04[c]	−0.04[c]	−0.07	0.03
δP	0.27	0.11	0.19	−0.11	−0.08
			1999		
E!	(0.90)	(0.90)	(0.92)	0.92[b]	0.92[b]
D!	(0.95)	(0.95)	(0.96)	0.96[b]	0.96[b]
δV	(−0.01)	(0.00)	(0.02)	−0.04	−0.03
δP	(−0.06)	(−0.22)	(−0.10)	0.08[d]	−0.02[d]
			2000		
E!	0.85	0.93	0.92	0.89	0.86
D!	0.95	0.97	0.97	0.95	0.95
δV	0.04	0.01	0.03	0.03	0.06
δP	−0.06	−0.16	−0.04	0.09	0.17
			2001		
E!	0.77[b]	0.92[b]	0.92[b]	0.90	0.88
D!	0.92[b]	0.96[b]	0.96[b]	0.96	0.95
δV	0.12[c]	0.02[c]	0.00[c]	0.10	0.12
δP	0.04	−0.10	0.02	−0.05	0.03
			All Years		
E!	0.84	0.90	0.91	0.89	0.87
D!	0.93	0.95	0.95	0.94	0.94
δV	0.00	0.00	0.00	0.00	0.01

[a] *D!* and *E!* were calculated at the hourly model time step. Values in parentheses indicate that the model was calibrated to 1999 streamflow for 240 Creek.
[b] Based on daily average flows where required due to data limitations.
[c] Calculated on reduced observation period due to data gaps.
[d] Based on recorded and simulated daily average peak.

canopy varies seasonally between $\tau_c = 0.18$ and 0.28, while the hemispherical canopy view factor controlling longwave fluxes to the forest snowpack is estimated at $V_f = 0.81 \pm 0.07$. DHSVM's original formulation for the forest radiation balance (scheme 1) was shown to overestimate shortwave transmittance ($\tau_c = 0.50$, season independent) and underestimate the view factor ($V_f = 0.50$) for the stand. An alternative formulation was adopted that is consistent with observed seasonal variations in canopy shortwave transmittance. Two end-member hypotheses regarding the impact of needle litter on forest snow albedo were tested within this new model formulation. The first (scheme 2) assumes that forest and clear-cut snow albedo are identical and requires a view factor $V_f = 1.7F$ to match the observed decline in melt-period forest SWE. The second hypothesis (scheme 3) considers the case where forest snow albedo is reduced compared to that in the clear-cut in adopting the *Whitaker et al.* [2003] curves and requires a view factor $V_f = 1.4F$ to match forest SWE measurements. It was found that model efficiency in reproducing 240 Creek streamflow for the 4-year period was improved slightly from 0.84 (scheme 1) to 0.90 for scheme 2 and to 0.91 for scheme 3 due to greater early-season snowmelt that results from the enhanced importance of longwave radiation below the forest canopy. Schemes 2 and 3 performed about equally well in simulating streamflow, reflecting parameter equifinality which can only be resolved by additional field measurements to ascertain preliminary data that suggest that the impact of needle litter on forest snow albedo may be limited. Nevertheless, the hypothesis testing confirmed the need for the revised forest radiation balance even if forest snow albedo is in fact lower than that in clear-cuts.

[46] Additional analyses revealed that the model is able to capture differences in canopy rainfall interception between small and large storms, tree transpiration over a 6-day summer period, and differences in soil moisture levels between a dry and a wet summer. While the model was calibrated to 1999 SWE and hydrograph data for the untreated 240 Creek basin, it successfully simulates forest and clear-cut SWE and streamflow in the three other years for this basin. It also successfully simulates without parameter adjustment observed hydrograph sensitivity to the more southerly aspect and greater stream network density of the treated 241 Creek basin as compared with 240 Creek. The results of this study demonstrate the ability of the modified DHSVM to capture many of the crucial hydrologic responses of the 240 and 241 Creek catchments over a 4-year preharvesting and postharvesting period. This is an encouraging performance and together with the Redfish Creek study [*Whitaker et al.*, 2003]

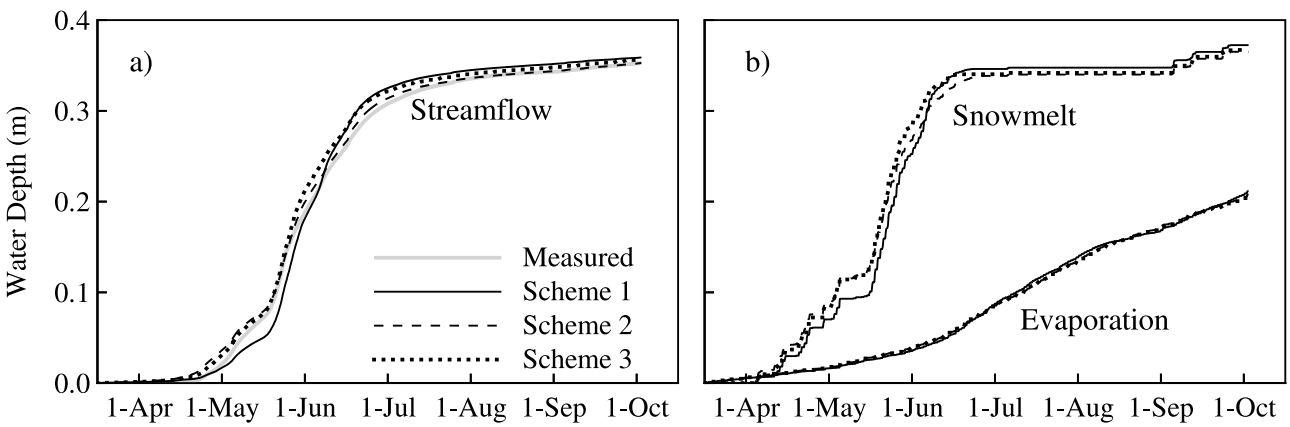

Figure 14. Comparison of 240 Creek simulation results for water year 2000 and the three radiation balance schemes: (a) streamflow accumulation and (b) basin-aggregated snowmelt and evaporation. Measured streamflow accumulation is shown for comparison.

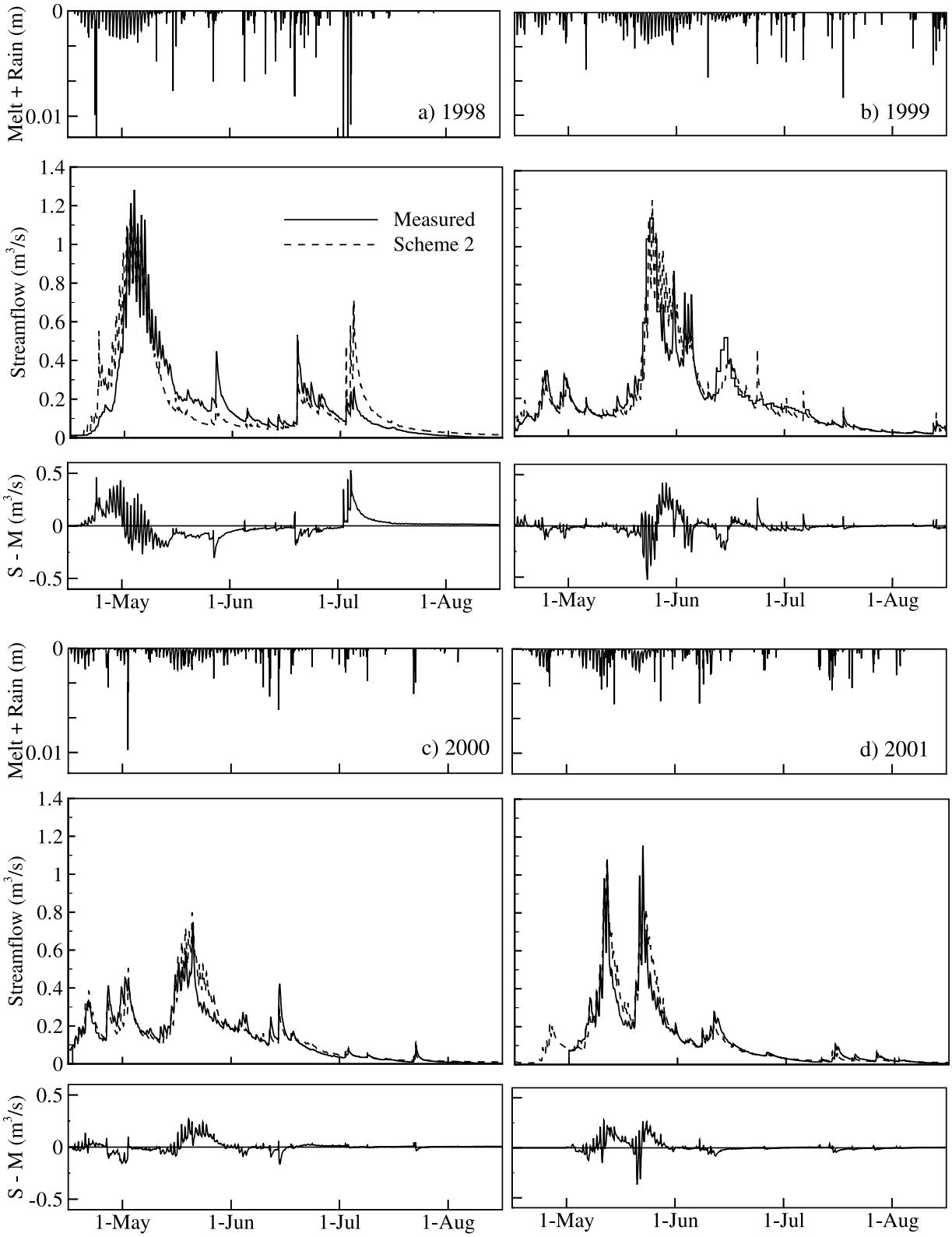

Figure 15. Measured (M) and scheme 2 simulated (S) streamflow for 241 Creek, together with residual time series S-M and simulated basin-aggregated snowmelt plus rainfall at hourly model time step. Results for scheme 3 are very similar. For parts of 1999 only daily-average flows were available.

suggests that the model may provide a reliable numerical tool for assessing changes in watershed processes due to forestry activities in the snowmelt-dominated interior regions of the Pacific Northwest.

[47] **Acknowledgments.** This work was funded by Forest Innovation Investment grant R02-15 to Y. Alila. Forest Renewal BC and the BC Forest Service funded collection and analysis of the Upper Penticton Creek data. The authors acknowledge the ongoing commitment of the Okanagan Shuswap Forest District and Weyerhaeuser Company Ltd. to research at UPC. Constructive comments by the anonymous reviewers helped improve the quality of the manuscript.

References

Adams, R. S., T. A. Black, and R. L. Fleming (1991), Evapotranspiration and surface conductance in a high elevation, grass covered forest clearcut, *Agric. For. Meteorol.*, *56*, 173–293.

Adams, R. S., D. L. Spittlehouse, and R. D. Winkler (1998), The snowmelt energy balance of a clearcut, forest and juvenile stand, in *Proceedings of the 23rd Conference on Agricultural Forest Meteorology, Albuquerque, NM, Nov. 2–6*, pp. 54–57, Am. Meteorol. Soc., Boston, Mass.

Alila, Y., and J. Beckers (2001), Using numerical modelling to address hydrologic forest management issues in British Columbia, *Hydrol. Processes*, *15*, 3371–3387.

Anderson, E. A. (1968), Development and testing of snowpack energy balance equations, *Water Resour. Res.*, *4*(1), 19–37.

Barry, R., M. Prevost, J. Stein, and A. P. Plamondon (1990), Application of a snow cover energy and mass balance model in a balsam fir forest, *Hydrol. Processes*, *26*, 1079–1092.

Beven, K. J., and A. Binley (1992), The future of distributed models: Model calibration and uncertainty prediction, *Hydrol. Processes*, *6*, 279–298.

Blöschl, G., D. Gutknecht, and R. Kirnbauer (1991), Distributed snowmelt simulations in an alpine catchment: 2. Parameter study and model predictions, *Water Resour. Res.*, *27*(12), 3181–3188.

Bowling, L., P. Storck, and D. Lettenmaier (2000), Hydrologic effects of logging in western Washington, United States, *Water Resour. Res.*, *36*(11), 3223–3240.

Burges, S. J. (2003), Process representation, measurements, data quality, and criteria for parameter estimation of watershed models, in *Calibration of Watershed Models*, *Water Sci. Appl. Ser.*, vol. 6, edited by Q. Duan et al., pp. 283–299, AGU, Washington, D. C.

Campbell, G. S., and J. M. Norman (1998), *An Introduction to Environmental Biophysics*, 2nd ed., Springer-Verlag, New York.

Entekhabi, D., and P. S. Eagleson (1989), Land surface hydrology parameterization for atmospheric general circulation models: Inclusion of subgrid scale spatial variability and screening with a simple climate model, *Ralph M. Parsons Lab. Rep. 325*, Mass. Inst. of Technol., Cambridge.

Gan, T. Y., and S. J. Burges (1990a), An assessment of a conceptual rainfall-runoff model's ability to represent the dynamics of small hypothetical catchments: 1. Models, model properties, and experimental design, *Water Resour. Res.*, *26*(7), 1595–1604.

Gan, T. Y., and S. J. Burges (1990b), An assessment of a conceptual rainfall-runoff model's ability to represent the dynamics of small hypothetical catchments: 2. Hydrologic responses for normal and extreme rainfall, *Water Resour. Res.*, *26*(7), 1605–1619.

Grayson, R. B., I. D. Moore, and T. A. McMahon (1992), Physically based hydrologic modeling: 2. Is the concept realistic?, *Water Resour. Res.*, *28*(10), 2659–2666.

Hardy, J. P., R. E. Davis, R. Jordan, X. Li, C. E. Woodcock, W. Ni, and J. C. McKenzie (1997), Snow ablation modeling at the stand scale in a boreal jack pine forest, *J. Geophys. Res.*, *102*(D24), 29,367–29,405.

Hardy, J. P., R. Melloh, P. Robinson, and R. Jordan (2000), Incorporating effects of forest litter in a snow process model, *Hydrol. Processes*, *13*, 3227–3237.

Hetherington, E. D. (1995), Subsurface water flow rates over bedrock on steep slopes in the Carnation Creek experimental watershed, in *Mountain Hydrology: Peaks and Valleys in Research and Application—Proceedings of the Canadian Water Resources Association Conference*, edited by B. T. Guy and J. Barnard, pp. 17–21, Can. Water Resour. Assoc., Cambridge, Ont., Canada.

Hope, G. (2001), Soil descriptions for Penticton Creek experimental watersheds, report, 19 pp., B. C. Minist. of For., Kamloops Reg., Kamloops, B. C., Canada.

Jakubauskas, M. E. (1996), Thematic mapper characterization of lodgepole pine seral stages in Yellowstone National Park, USA, *Remote Sens. Environ.*, *56*, 118–132.

James, L. D., and S. J. Burges (1982), Selection, calibration, and testing of hydrologic models, in *Hydrologic Modeling of Small Watersheds*, *Hydrol. Model. Monogr.*, vol. 5., edited by C. T. Haan, H. P. Johnson, and D. L. Brakensiek, pp. 437–472, Am. Soc. of Agric. Eng., St. Joseph, Mo.

Kollenberg, C. L., and K. L. O'Hara (1999), Leaf area and tree increment dynamics of even-aged and multi-aged lodgepole pine stands in Montana, *Can. J. For. Res.*, *29*, 687–695.

Kuczera, G. (1994), NLFIT: A Bayesian nonlinear regression program suite, 123 pp., Dep. of Civ. Eng. and Surv., Univ. of Newcastle, Newcastle, Australia.

Laramie, R. L., and J. C. J. Schaake (1972), Simulation of the continuous snowmelt process, report, Mass. Inst. of Technol., Cambridge.

Law, B. E., S. V. Tuyl, A. Cesscatti, and D. D. Baldocchi (2001), Estimation of leaf area index in open-canopy ponderosa pine forests at different successional stages and management regimes in Oregon, *Agric. For. Meteorol.*, *108*, 1–14.

Monteith, J. L., and M. H. Unsworth (1990), *Principles of Environmental Physics*, 2nd ed., Edward Arnold, London.

Nash, J. E., and J. V. Sutcliffe (1970), River flow forecasting through conceptual models, part I, A discussion of principles, *J. Hydrol.*, *10*, 282–290.

Pomeroy, J. W., and K. Dion (1996), Winter radiation extinction and reflection in a boreal pine canopy: Measurements and modelling, *Hydrol. Processes*, *10*, 1591–1608.

Rawls, W. J., L. R. Ahuja, D. L. Brakensiek, and S. Shirmohammadi (1993), Infiltration and soil water movement, in *Handbook of Hydrology*, pp. 5.1–5.51, edited by D. Maidment, McGraw-Hill, New York.

Reifsnyder, W. E., and H. W. Lull (1965), Radiant energy in relation to forests, *USDA For. Serv. Tech. Bull.*, *1344*, 111.

Smith, M. (1984), An ecological classification of the three sub-basins in the Penticton Creek watershed in the Englemann spruce subalpine fir zone, B.S. thesis, Fac. of For., Univ. of B. C., Vancouver, B. C., Canada.

Spittlehouse, D. L. (1998), Rainfall interception in young and mature conifer forests in British Columbia, in *Proceedings of the 23rd Conference on Agricultural and Forest Meteorology*, pp. 171–174, Am. Meteorol. Soc., Boston, Mass.

Spittlehouse, D. L. (2000), Using time domain reflectometry in stony forest soil, *Can. J. Soil Sci.*, *80*, 3–11.

Spittlehouse, D. L. (2002), Sap flow in old lodgepole pine trees, in *Proceedings of the 25th Conference on Agricultural and Forest Meteorology*, pp. 123–124, Am. Meteorol. Soc., Boston, Mass.

Spittlehouse, D. L., and R. D. Winkler (2002), Modelling snowmelt in a forest and clearcut, in *Proceedings of the 25th Conference on Agricultural and Forest Meteorology*, pp. 121–122, Am. Meteorol. Soc., Boston, Mass.

Storck, P. (2000), Trees, snow and flooding: An investigation of forest canopy effects on snow accumulation and melt at the plot and watershed scales in the Pacific Northwest, Dep. of Civ. Eng., Univ. of Wash., Seattle.

Storck, P., L. Bowling, P. Wetherbee, and D. Lettenmaier (1998), Application of a GIS-based distributed hydrology model for prediction of forest harvest effects on peak streamflows in the Pacific Northwest, *Hydrol. Processes*, *12*, 889–904.

Storck, P., D. P. Lettenmaier, and S. M. Bolton (2002), Measurement of snow interception and canopy effects on snow accumulation and melt in a mountainous maritime climate, Oregon, United States, *Water Resour. Res.*, *38*(11), 1223, doi:10.1029/2002WR001281.

Thomas, R. B., and W. F. Megahan (1998), Peak flow responses to clearcutting and roads in small and large basins, western Cascades, Oregon: A second opinion, *Water Resour. Res.*, *34*(12), 3393–3403.

Vertessey, R. A., F. G. R. Watson, and S. K. O'Sullivan (2001), Factors determining relations between stand age and catchment water balance in mountain ash forests, *For. Ecol. Manage.*, *143*, 13–26.

Waring, R. H., and J. F. Franklin (1979), Evergreen coniferous forests of the Pacific Northwest, *Science*, *204*, 1380–1386.

Whitaker, A., Y. Alila, J. Beckers, and D. Toews (2002), Evaluating peak flow sensivitiy to clear-cutting in different elevation bands of a snowmelt-dominated mountainous catchment, *Water Resour. Res.*, *38*(19), 1172, doi:10.1029/2001WR000514.

Whitaker, A., Y. Alila, J. Beckers, and D. Toews (2003), Application of the distributed hydrology soil vegetation model to Redfish Creek, British

Columbia: Model evaluation using internal catchment data, *Hydrol. Processes*, *17*, 199–224.

Wigmosta, M. S., L. W. Vail, and D. P. Lettenmaier (1994), A distributed hydrology-vegetation model for complex terrain, *Water Resour. Res.*, *30*(6), 1665–1679.

Wigmosta, M. S., B. Nijssen, and P. Storck (2002), The distributed hydrology soil vegetation model, in *Mathematical Models of Small Watershed Hydrology and Applications*, edited by V. P. Singh and D. K. Frevert, pp. 7–42, Water Resour. Publ., Highlands Ranch, Colo.

Winkler, R. D. (2001), The effects of forest structure on snow accumulation and melt in south-central British Columbia, Ph.D. thesis, Dep. of For. Resour. Manage., Univ. of B. C., Vancouver, B. C., Canada.

Winkler, R. D., D. L. Spittlehouse, B. A. Heise, T. L. Giles, and Y. Alila (2003), The Upper Penticton Creek Watershed Experiment: A review at year 20, in *Water Stewardship: How Are We Managing?—Proceedings of the Canadian Water Resources Association 56th Annual Conference*, pp. 51–58, Can. Water Resour. Assoc., Cambridge, Ont., Canada.

Wu, A., T. A. Black, D. L. Verseghy, P. D. Blanken, M. D. Novak, W. Chen, and P. C. Yang (2000), A comparison of parameterizations of canopy conductance of aspen and Douglas fir forests for CLASS, *Atmos. Ocean*, *38*, 81–112.

Y. Alila, J. Beckers, and M. Thyer, Department of Forest Resources Management, University of British Columbia, 2045–2424 Main Mall, Vancouver, BC, Canada, V6T 1Z4. (alila@interchange.ubc.ca; jbeckers@alumni.uwaterloo.ca; mark.thyer@tonkin.com.au)

D. Spittlehouse, British Columbia Ministry of Forests, Research Branch, 712 Yates Street, Victoria, B. C., Canada, V8W 1L4. (dave.spittlehouse@gems7.gov.bc.ca)

R. Winkler, British Columbia Ministry of Forests, Forest Sciences Section, Southern Interior Region, 515 Columbia Street, Kamloops, B. C., Canada, V2C 2T7. (rita.winkler@gems7.gov.bc.ca)